1989ApJ...342..558K

THE ASTROPHYSICAL JOURNAL, 342:558–575, 1989 July 1
© 1989. The American Astronomical Society. All rights reserved. Printed in U.S.A.

NONLINEAR INTERACTIONS AMONG SOLAR ACOUSTIC MODES

PAWAN KUMAR
High Altitude Observatory, National Center for Atmospheric Research[1]
AND
PETER GOLDREICH
California Institute of Technology
Received 1988 August 15; accepted 1988 December 14

ABSTRACT

We evaluate the rates at which nonlinear interactions transfer energy among the normal modes of a plane-parallel, stratified atmosphere. The atmosphere resembles the outer part of the Sun including the convection zone and the optically thin region above the photosphere up to the temperature minimum. The acoustic modes are assigned energies such that their photospheric velocities match those of the Sun's *p*-modes. The nonlinearity parameter is the acoustic Mach number, M, the ratio of the total acoustic velocity due to all of the modes to the sound speed. For $M^2 \ll 1$ the leading nonlinear interactions are those which couple three-modes. We show that every *p*-mode in the 5 minute band is involved in many near-resonant triplets. As a consequence, the energy transfer rates are independent of the mode line widths. Because M increases with height, the dominant contributions to the three-mode coupling coefficients occur in the upper part of the convection zone and in the optically thin isothermal layer. Moreover, the coupling coefficients tend to increase with ω and $\boldsymbol{k}_h$.

Nonlinear interactions which couple two trapped modes and one propagating mode drain energy from the trapped modes. They are far more effective than interactions among three trapped modes which drive the modes toward equipartition of energy. Thus, every trapped mode suffers a net loss of energy due to its nonlinear interactions. Estimates of the nonlinear energy transfer rates are plagued by two uncertainties. Some of the coefficients which couple two trapped modes to a propagating mode formally diverge as the thickness of the isothermal layer is increased to infinity; physically, this reflects the exponential growth of the acoustic Mach number with height in the isothermal layer. Also, the energy transfer rates are sensitive to the unknown energies of the high-degree trapped modes. Plausible assumptions lead to energy transfer rates which are somewhat smaller than the products of the mode energies and line widths. Thus, nonlinear mode coupling is probably not the dominant damping process for the solar *p*-modes, at least for those with small l. However, this cannot be regarded as a secure conclusion. The observational signature of damping due to nonlinear mode coupling would be a decrease in the energy per mode with increasing l at fixed ω. In addition, it might be responsible, at least in part, for the steep decline in the energy per mode at frequencies above 3 mHz which is usually attributed to radiative damping.

Our investigation indirectly bears on the question of the stability of the *p*-modes. We find that nonlinear mode couplings cannot limit the growth of overstable *p*-modes. This favors the hypothesis that the Sun's *p*-modes are stochastically excited by turbulent convection.

Subject headings: convection — Sun: atmosphere — Sun: atmospheric motions — Sun: oscillations

I. INTRODUCTION

In this paper we develop a method for evaluating nonlinear interactions among acoustic modes. We apply our method to calculate the rates of energy transfer among the normal modes of a plane-parallel model atmosphere. The properties of the atmosphere and the energies of the modes are chosen to resemble those of the Sun. These rates are then compared to the mode lifetimes to assess whether nonlinear interactions play a significant role in establishing the mode energies. The investigation is motivated by our desire to identify the mechanism by which the solar *p*-modes are excited.

The total velocity associated with solar oscillations is subsonic; the acoustic Mach number $M \lesssim 0.1$ everywhere below the photosphere. Since the nonlinearity parameter, M, is small, we treat the mode interactions via perturbation theory and retain only the lowest order terms. These couple triplets of modes.

We assume that the modes have random phases. The initial justification for this assumption is that each mode is coupled to many pairs of modes and no single coupling dominates its total interaction. A stronger case for random phases follows a conclusion of our study which is that nonlinear interactions make only a small contribution to the mode line widths. Other damping mechanisms, presumably some mix of radiative and turbulent dissipation, dominate the phase fluctuations of the modes. Since these forms of line broadening act independently on different modes they maintain random phases.

Our investigation is aimed at calculating the nonlinear interactions among all of the solar modes and evaluating their effects on limiting the amplitudes of overstable modes. In this respect it differs from previous work on nonlinear mode coupling in stars which focused on the interactions among only a few modes (e.g., Dziembowski 1982; Wentzel 1987).

[1] The National Center for Atmospheric Research is sponsored by the National Science Foundation.

© American Astronomical Society • Provided by the NASA Astrophysics Data System

1989ApJ...342..558K

TABLE 1

ATMOSPHERIC PARAMETERS

Parameter	Top of Adiabatic Atmosphere	Bottom of Adiabatic Atmosphere
z (cm)	2.85×10^7	3.38×10^{10}
P(g cm^{-1} s^{-2})	6.20×10^4	3.0×10^{12}
ρ(g cm^{-3})	1.96×10^{-7}	8.0×10^{-3}
g	2.775×10^4 cm s^{-2}	2.775×10^4 cm s^{-2}
ν_{crit}	5.069 mHz	5.069 mHz
Γ	5/3	5/3

NOTE.—ν_{crit} is the acoustic cutoff frequency for $k_h = 0$.

The paper is organized as follows. In § II we describe the plane-parallel atmosphere and the properties of its acoustic modes. We apply a Hamiltonian method, outlined in the Appendix, to derive the lowest order nonlinear interactions, the three-mode couplings, in § III. Section IV outlines the main features of the numerical procedure we use to calculate the rates at which three-mode interactions transfer energy among the normal modes. We compare these calculated rates to the observed line widths and explore the implications of this comparison for identifying the excitation mechanism of the solar p-modes, in § V.

II. NORMAL MODES OF THE MODEL ATMOSPHERE

Our computations are performed for a plane-parallel atmosphere that has horizontal cross-sectional area, A, and is enclosed between rigid vertical walls. Ultimately, we take the limit $A \to \infty$. The atmosphere sits in a uniform gravitational field and is composed of two layers, the lower adiabatic and the upper isothermal. The thermodynamic variables, pressure, density, and temperature, are continuous across the interface between the two layers. However, the density gradient is not. The adiabatic index, Γ, is set equal to 5/3 in both layers. The atmospheric parameters are listed in Table 1. They are chosen so that the atmosphere resembles the region of the Sun between the bottom of the convection zone and the temperature minimum. Except for its top few scale heights, the solar convection zone is nearly adiabatic, and the optically thin region above the solar photosphere may be crudely represented as isothermal. However, the upper part of the Sun's convective envelope possesses both a superadiabatic region and ionization zones of which our model atmosphere takes no account.

We take the vertical coordinate, z, to increase in the direction of the gravitational acceleration, $\boldsymbol{g}$, from $z = z_t$ at the interface between the two layers to $z = z_b$ at the bottom of the adiabatic zone. Because the unperturbed atmosphere is both static and plane-parallel, all of the variables associated with the modes depend on x, y, and t as $\exp i(\boldsymbol{k}_h \cdot \boldsymbol{x} - \omega t)$, where $\boldsymbol{k}_h$ is the horizontal wave vector and ω is the radian frequency.[2] We adopt the Eulerian enthalpy perturbation, $Q = p_1/\rho_0$, where p_1 is the Eulerian pressure perturbation and ρ_0 is the unperturbed density, as the dependent variable in the wave equation.

In the adiabatic atmosphere the linear wave equation reads

$$\frac{d^2Q}{dz^2} + \frac{3}{2z}\frac{dQ}{dz} + \left(\frac{\omega^2}{c^2} - k_h^2\right)Q = 0 , \tag{1}$$

where the adiabatic sound speed, c, satisfies $c^2 = 2gz/3$. The displacement vector, $\boldsymbol{\xi}$, is related to Q by

$$\xi_h = i\frac{\boldsymbol{k}_h Q}{\omega^2} , \qquad \xi_z = \frac{1}{\omega^2}\frac{dQ}{dz} . \tag{2}$$

The solution of equation (1) which is regular at $z = 0$ is a confluent hypergeometric function (Spiegel and Unno 1962; Christensen-Dalsgaard 1980). Changing the independent variable from z to $x = z^{1/2}$ transforms equation (1) into

$$\frac{d^2Q}{dx^2} + \frac{2}{x}\frac{dQ}{dx} + \left(\frac{6\omega^2}{g} - 4k_h^2 x^2\right)Q = 0 , \tag{3}$$

which reduces to the differential equation for spherical Bessel functions of zeroth order in the limit $k_h \to 0$. It is a classic example of a differential equation with two turning points. A simple WKB analysis yields the approximate analytic solution

$$Q \propto \frac{1}{z^{1/2}} \exp i\left[\int^z dz' k_z(z') + \delta\right] , \tag{4}$$

where δ is a constant phase which is determined by the boundary conditions, and

$$k_z(z) = \sqrt{\frac{3\omega^2}{2gz} - k_h^2} . \tag{5}$$

The upper and lower turning points are at

$$z_1 \approx \frac{2g}{3\omega^2} , \tag{6}$$

[2] The magnitude of $\boldsymbol{k}_h$ is related to the angular order, l, of the corresponding solar mode by $k_h R_\odot = l$.

© American Astronomical Society • Provided by the NASA Astrophysics Data System

1989ApJ...342..558K

and

$$z_2 \approx \frac{3\omega^2}{2gk_h^2} . \tag{7}$$

Between the turning points, $z_1 < z < z_2$,

$$\frac{k_z}{k_h} \approx \sqrt{\frac{z_2}{z} - 1} , \tag{8}$$

and the WKB *envelopes* of the components of $\boldsymbol{\xi}$ satisfy

$$\xi_h \propto \frac{1}{z^{1/2}} , \qquad \xi_z \propto \frac{1}{z} . \tag{9}$$

From equations (2) and (8) we see that ξ_z is the dominant component of $\boldsymbol{\xi}$ except very close to the lower turning point.

In the isothermal atmosphere linear, adiabatic wave propagation is governed by

$$\frac{d^2Q}{dz^2} + \frac{5g}{3c_0^2}\frac{dQ}{dz} + \left(\frac{\omega^2}{c_0^2} - k_h^2 + \frac{2g^2k_h^2}{3c_0^2\omega^2}\right)Q = 0 , \tag{10}$$

where c_0 is the adiabatic sound speed.[3] The displacement vector, $\boldsymbol{\xi}$, is related to Q by

$$\boldsymbol{\xi}_h = i\frac{\mathbf{k}_h Q}{\omega^2} , \qquad \xi_z = \left(\omega^2 - \frac{2g^2}{3c_0^2}\right)^{-1}\left(\frac{dQ}{dz} + \frac{2g}{3c_0^2}Q\right) . \tag{11}$$

The differential equation (10) has constant coefficients so it may be solved analytically. At each value of k_h, the acoustic cutoff frequency, $\omega_{ac}(k_h)$, separates the low-frequency, evanescent solutions from the high-frequency, propagating solutions. Expressed in terms of the scale height,

$$H = \frac{3c_0^2}{5g} , \tag{12}$$

the relation for ω_{ac} reads

$$\left(\frac{2\omega_{ac}H}{c_0}\right)^2 = \frac{1}{2}\left\{[1 + (2k_hH)^2] + \sqrt{[1 + (2k_hH)^2]^2 - \frac{96}{25}(2k_hH)^2}\right\} . \tag{13}$$

As the above equation shows, ω_{ac} increases with increasing k_h, but its dependence on k_h is weak for $k_hH \ll 1$, and in this limit equation (13) simplifies to $\omega_{ac} \approx c_0/2H = 5g/(6c_0)$. For $\omega < \omega_{ac}$ both solutions of equation (10) grow exponentially with height with inverse scale lengths given by

$$\kappa_\pm H = \frac{1}{2}\left\{1 \pm \sqrt{1 - \left(\frac{2\omega H}{c_0}\right)^2 + (2k_hH)^2\left[1 - \frac{24}{25}\left(\frac{c_0}{2\omega H}\right)^2\right]}\right\} . \tag{14}$$

The more slowly growing solution is the appropriate one for evanescent disturbances which originate within the adiabatic layer. For $k_hH \ll 1$ the expression for $\kappa_- H$ simplifies to

$$\kappa_- H \approx \frac{1}{2}\left[1 - \sqrt{1 - \left(\frac{\omega}{\omega_{ac}}\right)^2}\right] . \tag{15}$$

The propagating solutions of equation (10) also grow exponentially with height and have imaginary value of $k_zH = \frac{1}{2}$ as required by flux conservation.

The eigenfunctions are obtained by numerically integrating equation (1) through the adiabatic layer and then by matching the solutions to the analytic solutions of equation (10) in the isothermal layer. At $z = z_b$, we take $\xi_z = 0$. The boundary conditions at $z = z_t$ express the continuity of both ξ_z and the Lagrangian pressure perturbation, Δp. The latter condition is equivalent to the continuity of $Q + g\xi_z$. Thus, ξ_z, Q, and $\boldsymbol{\xi}_h$ are all continuous across $z = z_t$.

Trapped modes correspond to evanescent solutions in the isothermal layer. This restricts ω^2 to a discrete set of eigenfrequencies. We often use the number of nodes, n, in the vertical displacement eigenfunction instead of ω to identify a trapped mode for fixed k_h. The eigenfunctions for trapped modes are normalized such that

$$\omega_\alpha^2 \int_{-\infty}^{z_b} dz\, \rho_0\, \boldsymbol{\xi}_{k_h,n} \cdot \boldsymbol{\xi}^*_{k_h,m} = \delta_{n,m} . \tag{16}$$

We define the mass per unit surface area for a trapped mode α to be the ratio of its energy per unit surface area to its mean square

[3] The Brunt-Väisälä frequency, $N^2 = 2g^2/3c_0^2$.

© American Astronomical Society • Provided by the NASA Astrophysics Data System

1989ApJ...342..558K

surface velocity:

$$\mathcal{M}_\alpha \equiv \frac{1}{\omega_\alpha^2 |\xi_\alpha(z_s)|^2}, \tag{17}$$

where z_s is the surface value of z. Since $|\xi_\alpha(z)|$ grows exponentially with height in the isothermal layer, $\mathcal{M}_\alpha$ decreases exponentially with the height of the level at which the surface velocity is defined. The sensitivity of $\mathcal{M}_\alpha$ to height is small for $\omega \ll \omega_{ac}$ and increases monotonically with ω. The p-mode masses derived from our model atmosphere, $4\pi R_\odot^2 \mathcal{M}_\alpha$ are slightly larger at low l and slightly smaller at high l than those derived from a standard solar model. The modal masses track the solar ones fairly well as ω varies in spite of the limitations of the model atmosphere in representing the Sun.

The propagating modes are chosen to have no net flux in the isothermal layer; that is, they are composed of a pair of inward and outward propagating waves of equal amplitude. This choice ensures that they have real frequencies, are orthogonal to the trapped modes, and take on all frequencies $\omega \geq \omega_{ac}$. Propagating modes are normalized such that

$$\omega^2 \int_{-\infty}^{z_b} dz\, \rho_0\, \boldsymbol{\xi}_{\boldsymbol{k}_h,\omega} \cdot \boldsymbol{\xi}_{\boldsymbol{k}_h,\omega'} = \delta(\omega - \omega') . \tag{18}$$

The contribution from the adiabatic atmosphere to the integral in equation (18) is finite and thus negligible. The integration over the isothermal atmosphere may be carried out analytically to yield normalized enthalpy eigenfunctions for propagating modes in the isothermal atmosphere:

$$Q = C_\omega \sin [K_z(z - z_t) + \zeta_\omega] \exp\left[i\boldsymbol{k}_h \cdot \boldsymbol{x} - i\omega t + \frac{5(z - z_t)}{4z_t}\right], \tag{19}$$

with

$$K_z = \sqrt{\frac{\omega^2}{c_0^2} - k_h^2 + \frac{2g^2k_h^2}{3\omega^2c_0^2} - \frac{25g^2}{36c_0^4}},$$

$$C_\omega = \sqrt{\frac{2(3\omega^2c_0^2 - 2g^2)}{3\pi\rho_t K_z c_0^2 \omega}}, \tag{20}$$

where ρ_t is the density at the top of the adiabatic atmosphere and ζ_ω is determined by the continuity of ξ_z and Q at $z = z_t$.

It might seem more natural to adopt an outward radiation boundary condition for propagating modes in the isothermal atmosphere; we refer to these solutions as pseudomodes. Pseudomodes have discrete, complex frequencies. However, they are neither square integrable nor orthogonal to trapped modes. They correspond to resonances in the scattering amplitudes of incoming waves by the atmosphere. The normalized propagating modes reveal these resonances by having large amplitudes in the adiabatic atmosphere at frequencies equal to the real values of the frequencies of pseudomodes. With increasing $\omega > \omega_{ac}$ at fixed k_h these amplitudes exhibit a series of peaks. The location of each peak and its sharpness and height are related to the real and imaginary part of the frequency of a pseudomode. The observed power spectrum of solar p-modes at frequencies greater than ω_{ac} should contain broad peaks of width $\sim\omega/n$, where ω and n are the frequency and number of radial node of a pseudomode. Such pseudomodes have apparently been detected by Libbrecht (1988).

The $k_h - \omega$ diagram for the normal modes of the model atmosphere is displayed in Figure 1. It looks quite similar to that for the solar f- and p-modes except at small k_h where the finite depth of the adiabatic layer is responsible for changing the curvature of the dispersion ridges. The return to normal curvature is marked by the clustering of the ridges along a thin, almost vertical, line. For k_h sufficiently large that bottom effects are negligible, the dispersion curves are well fitted by the analytic formula

$$\omega^2 = \tfrac{4}{3}gk_h(n + \tfrac{3}{4}), \tag{21}$$

which is exact for an infinitely deep adiabatic atmosphere with vanishing surface pressure (Christensen-Dalsgaard 1980; Christensen Dalsgaard and Gough 1980).

A detailed comparison of the dispersion curves for the model atmosphere with those for the Sun reveals that, for $n > 0$ and large k_h, the former lie systemically above the latter.[4] This difference arises because, at depth, the temperature is lower at a given pressure in the Sun than in the model atmosphere; the lowering of the temperature gradient due to the reduction of Γ in the ionization zones more than compensates for the superadiabatic temperature gradient at the top of the convection zone in determining the run of temperature with depth in the Sun. The higher temperature of the model atmosphere leads to a higher sound speed and thus to higher frequency p-modes.

Expanding $\boldsymbol{\xi}$ in the terms of the normal modes of the system, we obtain

$$\boldsymbol{\xi} = \sum_\alpha \sqrt{\frac{\omega_\alpha J_\alpha}{2A}} [\boldsymbol{\xi}_\alpha(z) \exp(i\boldsymbol{k}_h \cdot \boldsymbol{x} - i\phi_\alpha) + \boldsymbol{\xi}_\alpha^*(z) \exp(-i\boldsymbol{k}_h \cdot \boldsymbol{x} + i\phi_\alpha)], \tag{22}$$

where J_α and ϕ_α are action-angle variables, and the sum over α is three-dimensional, two dimensions for $\boldsymbol{k}_h$, and one for ω. More

[4] Of course, the $n = 0$ curves are in excellent agreement because we have chosen the density at the top of the adiabatic layer of the model atmosphere to match that of the solar photosphere.

© American Astronomical Society • Provided by the NASA Astrophysics Data System

1989ApJ...342..558K

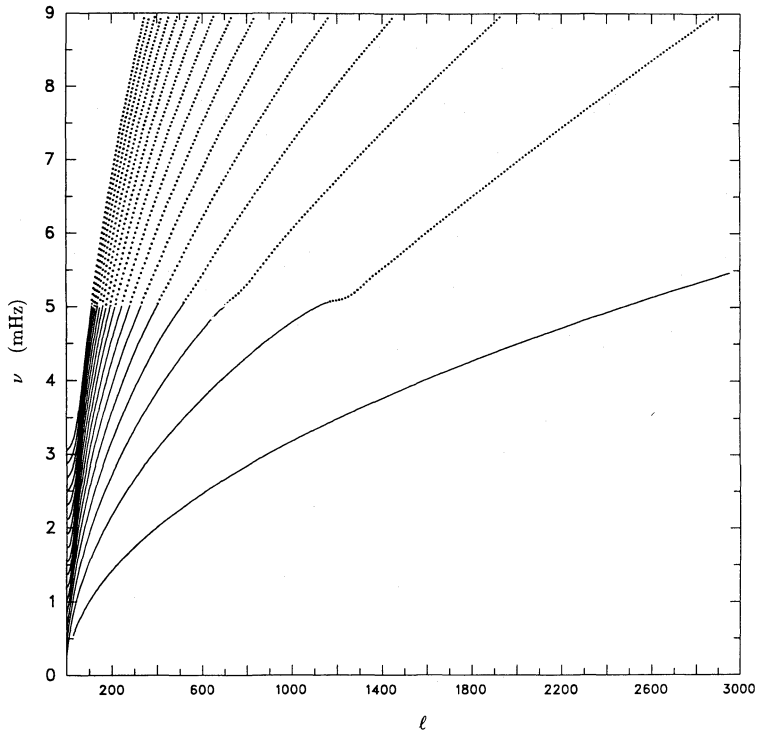

FIG. 1.—The $k_h - \omega$ diagram for the model atmosphere whose parameters are given in Table 1. Note that k_h has been multiplied by $R_\odot$, and the product is denoted by angular degree, l. Trapped modes are shown by solid lines and pseudomodes by dotted lines.

precisely, $\sum$ includes a sum over the discrete frequencies of the trapped modes and an integral over the continuous frequencies of the propagating modes. The phase $\phi_\alpha(t) = \omega_\alpha t + \epsilon_\alpha$.

III. THREE-MODE COUPLINGS

a) Hamiltonian Formalism

We adopt a Hamiltonian approach to the calculation of mode coupling. The Hamiltonian is expanded in powers of the displacement vector $\boldsymbol{\xi}$. The second-order terms yield the linear differential equations (1) and (10) for the normal modes, and the third-order terms describe nonlinear interactions among them. We assume that the nonlinear interactions are sufficiently weak so that they may be determined perturbatively. We assess this important approximation in § IV*d*.

The second- and third-order parts of the Hamiltonian density appropriate to the adiabatic perturbations of a static configuration composed of a perfect gas take the form (see Appendix A)

$$\mathscr{H} = \mathscr{H}_2 + \mathscr{H}_3 , \tag{23}$$

where

$$\mathscr{H}_2 = \frac{\rho_0}{2}\left(\frac{\partial \boldsymbol{\xi}}{\partial t}\right)^2 + \frac{p_0}{2}\left[(\Gamma - 1)(\nabla \cdot \boldsymbol{\xi})^2 + \xi^{i,j}\xi^{j,i}\right] , \tag{24}$$

and

$$\mathscr{H}_3 = -p_0\left[\frac{(\Gamma - 1)^2}{6}(\nabla \cdot \boldsymbol{\xi})^3 + \frac{(\Gamma - 1)}{2}(\nabla \cdot \boldsymbol{\xi})\xi^{i,j}\xi^{j,i} + \frac{1}{3}\xi^{i,j}\xi^{j,k}\xi^{k,i}\right] , \tag{25}$$

where p_0 is unperturbed pressure, $\xi^{i,j}$ is the derivative of ξ^i with respect to x^j, and the summation convention for repeated indices is assumed. We evaluate the three-mode couplings among the acoustic modes of the plane-parallel, stratified atmosphere described in the previous section. Expressing the second-order Hamiltonian density, $\mathscr{H}_2$, in the terms of the normal modes and integrating it over volume, we find

$$H_2 \equiv \int d^3x\, \mathscr{H}_2 = \sum_\alpha \omega_\alpha J_\alpha = \sum_\alpha E_\alpha . \tag{26}$$

Thus, the energy in mode α, $E_\alpha = \omega_\alpha J_\alpha$.

Next, we expand $\mathscr{H}_3$ in the terms of the normal modes and integrate it over space to obtain

$$H_3 \equiv \int d^3x\, \mathscr{H}_3 = \sum_{\alpha_{s\alpha},\, \beta_{s\beta},\, \gamma_{s\gamma}} \sqrt{\frac{E_\alpha E_\beta E_\gamma}{8A}}\, K_{\alpha_{s\alpha}\beta_{s\beta}\gamma_{s\gamma}} \exp\left[-i(s_\alpha \phi_\alpha + s_\beta \phi_\beta + s_\gamma \phi_\gamma)\right] . \tag{27}$$

© American Astronomical Society • Provided by the NASA Astrophysics Data System

1989ApJ...342..558K

The terms in the above sum are restricted by the conservation of horizontal momentum expressed through the matching condition on the horizontal wave vectors,

$$s_\alpha \boldsymbol{k}_{h\alpha} + s_\beta \boldsymbol{k}_{h\beta} + s_\gamma \boldsymbol{k}_{h\gamma} = 0 \,, \tag{28}$$

where α, β, γ refer to different modes of oscillation and the symbols $s_\alpha, s_\beta, s_\gamma$ take on the values $+1$ or -1.

The coefficient $K_{\alpha_{s\alpha}\beta_{s\beta}\gamma_{s\gamma}}$ which appears in equation (27) is symmetrical under the interchange of indices $\alpha_{s\alpha}$, $\beta_{s\beta}$, and $\gamma_{s\gamma}$. It is defined by

$$K_{\alpha_{s\alpha}\beta_{s\beta}\gamma_{s\gamma}} = -\int dz\, \frac{p_0}{6} \{(\Gamma - 1)^2 (\nabla \cdot \boldsymbol{\xi}_{\alpha_{s\alpha}})(\nabla \cdot \boldsymbol{\xi}_{\beta_{s\beta}})(\nabla \cdot \boldsymbol{\xi}_{\gamma_{s\gamma}}) + \xi^{i,j}_{\alpha_{s\alpha}} \xi^{j,k}_{\beta_{s\beta}} \xi^{k,i}_{\gamma_{s\gamma}} + \xi^{i,j}_{\beta_{s\beta}} \xi^{j,k}_{\alpha_{s\alpha}} \xi^{k,i}_{\gamma_{s\gamma}}$$
$$+ (\Gamma - 1)[(\nabla \cdot \boldsymbol{\xi}_{\alpha_{s\alpha}}) \xi^{i,j}_{\beta_{s\beta}} \xi^{j,i}_{\gamma_{s\gamma}} + (\nabla \cdot \boldsymbol{\xi}_{\beta_{s\beta}}) \xi^{i,j}_{\gamma_{s\gamma}} \xi^{j,i}_{\alpha_{s\alpha}} + (\nabla \cdot \boldsymbol{\xi}_{\gamma_{s\gamma}}) \xi^{i,j}_{\alpha_{s\alpha}} \xi^{j,i}_{\beta_{s\beta}}]\} \,, \tag{29}$$

where the complex conjugate eigenfunction should be used for $s_\mu = -1$.

Our system has now been reduced to that of N interacting harmonic oscillators with action-angle variables, J_α, ϕ_α. In terms of these variables the Hamiltonian reads

$$H = \boldsymbol{\omega} \cdot \boldsymbol{J} + H_{\rm int}(\boldsymbol{J}, \boldsymbol{\phi}) \,. \tag{30}$$

The Hamilton equations then yield

$$\frac{\partial \boldsymbol{\phi}}{\partial t} \equiv \dot{\boldsymbol{\phi}} = \frac{\partial H}{\partial \boldsymbol{J}} \,, \tag{31}$$

and

$$\frac{\partial \boldsymbol{J}}{\partial t} \equiv \dot{\boldsymbol{J}} = -\frac{\partial H}{\partial \boldsymbol{\phi}} \,. \tag{32}$$

Substituting for H_3 from equation (27) in the Hamilton equations (31) and (32), we find the evolution equations for mode α due to a single triplet:

$$\frac{d\phi_\alpha}{dt} = \omega_\alpha + \frac{6\omega_\alpha |K_{\alpha_{s\alpha}\beta_{s\beta}\gamma_{s\gamma}}|}{\sqrt{8A}} \sqrt{\frac{E_\beta E_\gamma}{E_\alpha}} \cos(\Phi + \delta_3) \,, \tag{33}$$

and

$$\frac{dJ_\alpha}{dt} = \frac{12 s_\alpha |K_{\alpha_{s\alpha}\beta_{s\beta}\gamma_{s\gamma}}|}{\sqrt{8A}} \sqrt{E_\alpha E_\beta E_\gamma} \sin(\Phi + \delta_3) \,, \tag{34}$$

where Φ and δ_3 are defined by

$$\Phi \equiv s_\alpha \phi_\alpha + s_\beta \phi_\beta + s_\gamma \phi_\gamma \,, \tag{35}$$

and

$$K_{\alpha_{s\alpha}\beta_{s\beta}\gamma_{s\gamma}} = |K_{\alpha_{s\alpha}\beta_{s\beta}\gamma_{s\gamma}}| \exp(i\delta_3) \,. \tag{36}$$

The combinatorial factors of 6 and 12 in equations (33) and (34) arise because the triplet (α, β, γ) occurs 6 times for each choice of α in equation (27).

b) *Master Equation*

For simplicity, we begin by calculating dE_α/dt due to the interactions among the single triplet (α, β, γ) and then sum the result over all possible triplets which involve mode α. Finally, we take the expectation value of the resulting expression to obtain the master equation which governs the expectation value of the rate at which nonlinear interactions change the energy of mode α.

We solve equations (33) and (34) perturbatively. The zeroth-order values of ϕ_α and J_α are taken to be the actual values at some arbitrarily chosen time t. The corrections of order n at time $t + \tau$ are computed with the right-hand sides of the equations evaluated to order $n - 1$. This procedure, carried out to first order for ϕ_α and to second order for J_α, yields

$$\phi^{(1)}_\alpha(t + \tau) = \frac{6\omega_\alpha |K_{\alpha_{s\alpha}\beta_{s\beta}\gamma_{s\gamma}}|}{\sqrt{8A}\,\Delta\omega} \sqrt{\frac{E^{(0)}_\beta E^{(0)}_\gamma}{E^{(0)}_\alpha}} [\sin(\Delta\omega\tau + \epsilon_3 + \delta_3) - \sin(\epsilon_3 + \delta_3)] \,, \tag{37}$$

$$J^{(1)}_\alpha(t + \tau) = -\frac{12 s_\alpha |K_{\alpha_{s\alpha}\beta_{s\beta}\gamma_{s\gamma}}|}{\sqrt{8A}\,\Delta\omega} \sqrt{E^{(0)}_\alpha E^{(0)}_\beta E^{(0)}_\gamma} [\cos(\Delta\omega\tau + \epsilon_3 + \delta_3) - \cos(\epsilon_3 + \delta_3)] \,, \tag{38}$$

and

$$J^{(2)}_\alpha(t + \tau) = \frac{18 |K_{\alpha_{s\alpha}\beta_{s\beta}\gamma_{s\gamma}}|^2}{A(\Delta\omega)^2} \sin^2\left(\frac{\Delta\omega\tau}{2}\right) [\omega_\alpha E^{(0)}_\beta E^{(0)}_\gamma + s_1 \omega_\beta E^{(0)}_\alpha E^{(0)}_\gamma + s_2 \omega_\gamma E^{(0)}_\alpha E^{(0)}_\beta] \,, \tag{39}$$

© American Astronomical Society • Provided by the NASA Astrophysics Data System

1989ApJ...342..558K

where

$$\epsilon_3 \equiv s_\alpha \epsilon_\alpha^{(0)} + s_\beta \epsilon_\beta^{(0)} + s_\gamma \epsilon_\gamma^{(0)} , \tag{40}$$

$$s_1 \equiv \frac{s_\beta}{s_\alpha} , \qquad s_2 \equiv \frac{s_\gamma}{s_\alpha} , \tag{41}$$

and

$$\Delta\omega \equiv s_\alpha \omega_\alpha + s_\beta \omega_\beta + s_\gamma \omega_\gamma \approx 0 . \tag{42}$$

We assume that the phases of different modes are uncorrelated and define

$$\left\langle \frac{dE_\alpha}{dt} \right\rangle \equiv \frac{\omega_\alpha}{\tau} J_\alpha^{(2)}(t+\tau) . \tag{43}$$

The angle brackets denoting expectation value are called for because we discard the direct contribution which $J_\alpha^{(1)}$ makes to dE_α/dt because it has vanishing expectation value.

Next, we substitute equation (39) into equation (43) and simplify the resulting expression by setting

$$\frac{1}{(\Delta\omega)^2} \sin^2\left(\frac{\Delta\omega\tau}{2}\right) \approx \frac{\pi\tau}{2} \delta(\Delta\omega) , \tag{44}$$

which is an expression of approximate energy conservation.

Then, we sum equation (43) over all the triplets which contain mode α and take the limit $A \to \infty$. The latter step involves the replacement

$$\lim_{A\to\infty} \frac{1}{A} \sum_{\boldsymbol{k}_{h\beta},\, \boldsymbol{k}_{h\gamma}} = \frac{1}{(2\pi)^4} \int d^2k_{h_\beta} d^2k_{h_\gamma} . \tag{45}$$

The horizontal wave vector matching condition given by equation (28) introduces a term $(2\pi)^2\delta(s_\alpha \boldsymbol{k}_{h\alpha} + s_\beta \boldsymbol{k}_{h\beta} + s_\gamma \boldsymbol{k}_{h\gamma})$ which reduces the double integal to a single one over $d^2k_{h_\beta}$. These steps lead to

$$\left\langle \frac{dE_{\boldsymbol{k}_{h\alpha}}}{dt} \right\rangle = \frac{9\omega_\alpha}{2\pi} \sum_{n_\beta} \int d\omega_\gamma \int dk_{h\beta}\, k_{h\beta} \int_0^\pi d\theta_{\alpha\beta} \, |K_{\alpha_{s\alpha}\beta_{s\beta}\gamma_{s\gamma}}|^2 \delta(\omega_\alpha + s_1\omega_\beta + s_2\omega_\gamma)(\omega_\alpha E_\beta E_\gamma + s_1\omega_\beta E_\alpha E_\gamma + s_2\omega_\gamma E_\alpha E_\beta) , \tag{46}$$

where $\theta_{\alpha\beta}$ is the angle between $\boldsymbol{k}_{h\alpha}$ and $\boldsymbol{k}_{h\beta}$. We note that $0 \le \theta_{\alpha\beta} < 2\pi$, and that $\theta_{\alpha\beta}$ and $2\pi - \theta_{\alpha\beta}$ correspond to the same value of $k_{h\gamma}$. To account for this degeneracy, we integrate over $d\theta_{\alpha\beta}$ from 0 to π and include a factor of 2 in equation (46).

The triplets with which we are concerned have at most one propagating mode, and it is always taken to be mode γ. We have written equation (46) in a form which is suitable for either a propagating or a trapped mode γ. In the former case, the integrand is a continuous function of ω_γ which exhibits peaks at the frequencies of the pseudomodes described in § II. A plot of $|K_{\alpha\beta\gamma}|$ as a function of k_γ showing these peaks is provided as Figure 2. In the latter case, the integral over $d\omega_\gamma$ reduces to a sum over n_γ.

If mode γ is propagating, the integral over ω_γ in equation (46) is carried out trivially to yield

$$\left\langle \frac{dE_{\boldsymbol{k}_{h\alpha}}}{dt} \right\rangle = \frac{9\omega_\alpha}{2\pi} \sum_{n_\beta} \int dk_{h\beta}\, k_{h\beta} \int_0^\pi d\theta_{\alpha\beta} \, |K_{\alpha_{s\alpha}\beta_{s\beta}\gamma_{s\gamma}}|^2 \{\omega_\alpha E_\beta E_\gamma + s_1\omega_\beta E_\alpha E_\gamma + s_2\omega_\gamma E_\alpha E_\beta\} . \tag{47}$$

If mode γ is trapped, we carry out the integral over $\theta_{\alpha\beta}$ and eliminate the δ-function in frequency using

$$d^2k_{h_\beta} = k_{h_\beta} dk_{h_\beta} d\theta_{\alpha\beta} = k_{h_\beta} \frac{d\theta_{\alpha\beta}}{d\omega_\gamma} dk_{h_\beta} d\omega_\gamma , \tag{48}$$

and

$$\cos\theta_{\alpha\beta} = s_1 \frac{k_{h\gamma}^2 - k_{h\alpha}^2 - k_{h\beta}^2}{2k_{h\alpha}k_{h\beta}} , \tag{49}$$

to arrive at

$$\frac{d\theta_{\alpha\beta}}{d\omega_\gamma} = \frac{-s_1 2k_{h\gamma}}{\sqrt{[(k_{h\alpha}+k_{h\beta})^2 - k_{h\gamma}^2][k_{h\gamma}^2 - (k_{h\alpha}-k_{h\beta})^2]}} \frac{dk_{h\gamma}}{d\omega_\gamma} . \tag{50}$$

Taken together, these operations on equation (46) yield the time rate of change of mean energy in mode α due to its couplings with all possible trapped modes

$$\left\langle \frac{dE_{\boldsymbol{k}_{h\alpha}}}{dt} \right\rangle = \frac{9\omega_\alpha}{\pi} \sum_{n_\beta,\, n_\gamma} \int dk_{h\beta} \frac{|K_{\alpha_{s\alpha}\beta_{s\beta}\gamma_{s\gamma}}|^2 k_{h\beta} k_{h\gamma}}{\sqrt{[(k_{h\alpha}+k_{h\beta})^2 - k_{h\gamma}][k_{h\gamma}^2 - (k_{h\alpha}-k_{h\beta})^2]}} \frac{dk_{h\gamma}}{d\omega_\gamma} (\omega_\alpha E_\beta E_\gamma + s_1\omega_\beta E_\alpha E_\gamma + s_2\omega_\gamma E_\alpha E_\beta) . \tag{51}$$

The expressions for $\langle dE_{\boldsymbol{k}_{h\alpha}}/dt \rangle$ given in equations (47) and (51) are the fundamental formulae of this paper. For each, it is

© American Astronomical Society • Provided by the NASA Astrophysics Data System

1989ApJ...342..558K

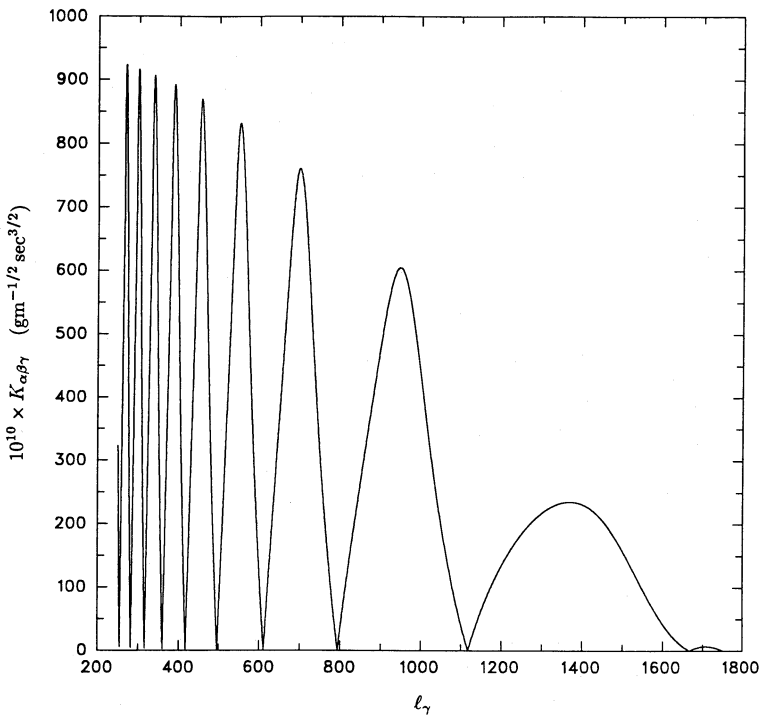

FIG. 2.—$|K_{\alpha\beta\gamma}|$ as a function of $k_{h\gamma}$ for fixed modes α ($l_\alpha = 1000$, $\nu_\alpha = 3.180$ mHz) and β ($l_\beta = 750$, $\nu_\beta = 2.754$ mHz)

important to avoid double counting modes in carrying out the integral over $k_{h\beta}$. The frequency matching equation (42) implies that either one or both of s_1 and s_2 are negative. In the former case we choose $s_2 = -1$ and take the integral over those modes for which $\omega_\gamma \geq \omega_\beta$. In the latter case, $s_1 = s_2 = -1$, the integral is restricted to modes with $\omega_\beta \leq \omega_\alpha/2$.

c) *Number of Resonant Triplets per Solar p-Mode*

In deriving the master equation for three trapped modes, we have implicitly assumed that each mode is involved in many triplets which satisfy the frequency matching equation (42) to within the sum of the line widths of the three modes. Otherwise, the steps taken in equations (44) and (45) which lead to an expression that is independent of the line widths could not be defended. We justify this procedure below.

Let us estimate the number of resonant triplets which involve a particular mode α. By a resonant triplet we mean one which satisfies the frequency matching condition given by equation (42) to within the sum of the line widths of the three modes. For simplicity, we consider a restricted set of couplings for which ω and l for all three modes (α, β, γ) lie within intervals $\Delta\omega/\omega_* \lesssim 1$ and $\Delta l/l_* \lesssim 1$ about the fiducial values ω_* and l_*.[5] Moreover, we assume that all the modes have similar line widths $\Delta\omega \approx \omega/\mathcal{Q}$, wnere $\mathcal{Q}$ is the quality factor.

Given mode α there are $N_\beta \sim n_* l_*^2$ choices for mode β.[6] With both α and β determined the angular momentum addition rules allow of order l_* possible choices of l for mode γ. However, for $l_* \gg 1$ one Clebsch-Gordon coupling coefficient is much larger than the others and l_γ is essentially unique.[7] Approximate energy conservation determines ω_γ to within a tolerance of order $\omega_*/\mathcal{Q}$. Thus, the probability that an appropriate mode γ exists to complete the resonant triple is $N_\gamma \sim n_*/\mathcal{Q}$. Multiplying this probability by the number of possible choices for mode β we obtain an estimate of

$$\mathcal{N} \equiv N_\beta N_\gamma \sim \frac{n_*^2 l_*^2}{\mathcal{Q}} \tag{52}$$

for the number of resonant triplets which involve mode α.

The solar p-modes in the 5 minute band have $\mathcal{Q} \sim 10^3$ and (n, l) combinations ranging from (25, 0) to (0, 10^3). As examples, we take the limiting cases $(n_*, l_*) = (20, 10)$ and $(n_*, l_*) = (1, 700)$. These choices yield $\mathcal{N} \sim 4 \times 10^1$ and $\mathcal{N} \sim 5 \times 10^2$, respectively. Thus, we may safely conclude that each 5 minute mode is coupled to many other modes.

IV. NUMERICAL PROCEDURE AND RESULTS

a) *Class 1 and Class 2 Triplets*

As is already clear from the last section, the three-mode couplings separate naturally into two classes.

Class 1 consists of all the possible triplets for which $\omega_\gamma \geq \omega_{ac}$. Since mode γ is propagating it has negligible energy. The three-mode coupling acts to drain energy from the trapped modes α and β. We denote by $\Upsilon_\alpha^{(1)}$ the rate at which mode α loses energy

[5] In the remainder of this subsection we use the radial order, n, instead of ω, together with l and m to specify a mode.
[6] For each (n, l) pair $-l \leq m \leq l$.
[7] For $l_* \gg 1$ the rules for the addition of l reduce to those for the addition of k_h.

© American Astronomical Society • Provided by the NASA Astrophysics Data System

1989ApJ...342..558K

as the result of its class 1 couplings. To compute $\Upsilon_\alpha^{(1)}$, we set $E_\gamma = 0$ and $s_2 = -1$ in equation (47) and sum over all the class 1 triplets which involve mode α.

Class 2 contains the remaining resonant triplets, those which involve only trapped modes. Each three-mode coupling in this class drives the modes it connects toward equipartition of energy. Since the trapped modes with frequencies just below ω_{ac} have the lowest energies, these interactions tend to transfer energy from the lower to the higher frequency modes. To compute $\Upsilon_\alpha^{(2)}$, the net rate at which three-mode couplings in class 2 change the energy of mode α, we sum the contributions to equation (51) over all those class 2 triplets which include mode α.

We note that $\Upsilon_\alpha^{(1)}$ is always negative, but $\Upsilon_\alpha^{(2)}$ may have either sign. In general, $\Upsilon_\alpha^{(1)}$ is much larger than $\Upsilon_\alpha^{(2)}$, for reasons explained in § IV*d*.

b) Mode Energies

Mode energies are required as input to the calculations of the energy transfer rates given by equations (47) and (51). Libbrecht and Zirin (1986) and Libbrecht (1988) have accurately measured the surface velocities of the low-degree, $l \lesssim 20$, solar p-modes in the 5 minute band. We determine mode energies by multiplying their mean square velocities by mode masses appropriate to the line-forming level for their observations. We adopt these mode energies for our calculations making the assumption that the mode energy is independent of l. While this assumption is theoretically plausible, its observational support is shaky. The most relevant high-degree, $l \lesssim 200$, results indicate that the rms surface velocities do not vary with l (Libbrecht *et al.* 1986). Since the mode mass decreases by about a factor of 3 between $l = 0$ and $l = 200$, there may be a slow decline in mode energy with increasing l. Our assumption of l-independent mode energy tends to overestimate the importance of nonlinear mode coupling if the mode energies really do decline with increasing l.

The total mean-square surface velocity is obtained by summing the contributions from all of the trapped modes. We have

$$v^2 \equiv \lim_{A\to\infty} \frac{1}{A} \int d^2x_h \left| \frac{\partial \xi}{\partial t} \right|^2 = \sum_{n_\alpha} \int \frac{d^2k_{h_\alpha}}{(2\pi)^2} \frac{E_\alpha}{M_\alpha} . \tag{53}$$

The mode energies we adopt yield $v_{rms} \approx 0.8$ km s^{-1} at the interface between the adiabatic and isothermal layers. At higher levels v_{rms} is larger; the precise value depends on the energies of the unobserved, high-degree, trapped modes.

c) Calculational Method

i) *Class 1 Triplets*

A straightforward numerical computation of $\Upsilon_\alpha^{(1)}$ involves a two-dimensional integral over $\boldsymbol{k}_{h\beta}$ since there is a propagating mode for all $\boldsymbol{k}_{h\gamma}$ and $\omega_\gamma \geq \omega_{ac}(k_h)$.

ii) *Class 2 Triplets*

Starting with mode α, we find all pairs of modes that satisfy the horizontal wavevector and frequency matching conditions given by equations (28) and (42). To do so, we slide the position of mode β along the portion of each ridge in the $k_h - \omega$ diagram which lies below the acoustic cutoff frequency, ω_{ac}. For specified values, k_{h_α}, ω_α and k_{h_β}, ω_β, the values of k_{h_γ}, ω_γ correspond to the intersections of the lines $\omega_\gamma = \omega_\alpha \pm \omega_\beta$ with the ridges in the $k - \omega$ diagram that lie between the boundaries $|k_{h\alpha} - k_{h\beta}| \leq k_{h\gamma} \leq k_{h\alpha} + k_{h\beta}$. The coupling coefficient for each triplet is computed using equation (29), and $\Upsilon_\alpha^{(2)}$ is obtained by summing the contributions from all the class 2 triplets which involve mode α.

d) Three-Mode Coupling Coefficients

Physically, we expect the nonlinear mode interaction to be strongest in regions where the appropriate nonlinearity parameter, viz., the acoustic Mach number, is large. Mathematically, the local contribution to the three-mode coupling coefficient is proportional to the product of the unperturbed pressure and the gradients of the displacement eigenfunctions of the three modes (see eq. [29]). Let us separate the contributions to $K_{\alpha\beta\gamma}$ from the adiabatic and isothermal layers and examine each individually.

The situation is simpler in the adiabatic layer and we begin with it. Here $p_0 \propto z^{5/2}$. The dominant term in gradient of the displacement is $\partial\xi_z/\partial z$, whose envelope diminishes as $z^{-3/2}$ for $z_1 < z < z_2$ and as $\exp(-k_h z)$ for $z > z_2$ (see eq. [9]). This gives a local three-mode coupling strength which decreases at least as fast as z^{-2} for z greater than the largest z_1 of the three modes. Thus, the contribution to the three-mode coupling coefficient from the adiabatic layer is concentrated close to its upper boundary.

Nonlinear mode coupling in the isothermal layer is complicated by the exponential increase with height of ξ (see eq. [15]) which, for some triplets, overwhelms the exponential decrease of the pressure in the integrand of the coupling coefficient. Coupling coefficients which formally diverge in an infinite isothermal atmosphere are primarily associated with class 1 triplets, especially those for which the frequency of at least one of the trapped modes is not far below the acoustic cutoff. A physically plausible way to bound the coupling coefficients is to choose the upper limit in their defining integral to be the height at which the acoustic Mach number reaches unity. Unfortunately, the validity of the perturbation expansion becomes questionable at this point; higher order couplings have comparable strengths to the three-mode couplings there.

Even the coefficients which are formally convergent show a pronounced increase in magnitude with increasing ω and k_h of the modes they couple. This dependence is due to the increased concentration of modes with high values of ω and k_h in the upper layers of the atmosphere. It is the same property that is responsible for the small masses of these modes (see Table 2). Furthermore, for small k_{h_α}, $k_{h_\beta} \sim k_{h_\gamma}$, and since the magnitude of $K_{\alpha\beta\gamma}$ is roughly proportional to $k_{h_\beta} k_{h_\gamma}$ (see eq. [29]), $K_{\alpha\beta\gamma}$ increases with increasing k_{h_β} as $k_{h_\beta}^2$. Of course, there is an upper limit to k_{h_β} beyond which the contribution to mode coupling declines rapidly. This turnover arises because the mode energy spectrum falls rapidly at high frequencies.

Figure 3 displays the integrand of the mode coupling coefficient for a variety of triplets.

© American Astronomical Society • Provided by the NASA Astrophysics Data System

1989ApJ...342..558K

TABLE 2

MODE PROPERTIES

ν (mHz)	P (minute)	$k_h R_\odot \equiv \ell$	n	M_α (gram)	E_α (erg)
1.1140	14.96	122.7	0	1.552×10^{26}	2.90×10^{26}
1.5914	10.47	250.4	0	2.897×10^{25}	2.90×10^{26}
1.7505	9.52	303.0	0	1.879×10^{25}	3.94×10^{26}
1.8620	8.95	342.8	0	1.426×10^{25}	5.70×10^{26}
1.9894	8.38	391.3	0	1.066×10^{25}	8.28×10^{26}
2.2282	7.48	490.9	0	6.569×10^{24}	1.66×10^{27}
2.3873	6.98	563.5	0	4.945×10^{24}	2.65×10^{27}
2.5463	6.55	641.1	0	3.819×10^{24}	4.26×10^{27}
2.7852	5.98	767.0	0	2.712×10^{24}	6.56×10^{27}
3.0239	5.51	904.1	0	2.022×10^{24}	9.37×10^{27}
3.1831	5.24	1001.8	0	1.703×10^{24}	9.68×10^{27}
3.3423	4.99	1104.5	0	1.462×10^{24}	6.79×10^{27}
3.5810	4.65	1267.9	0	1.201×10^{24}	3.07×10^{27}
3.7401	4.46	1383.1	0	1.078×10^{24}	1.61×10^{27}
3.9789	4.19	1565.3	0	9.471×10^{23}	7.91×10^{26}
4.3768	3.81	1894.0	0	8.426×10^{23}	3.07×10^{26}
4.6155	3.61	2106.3	0	8.468×10^{23}	1.75×10^{26}
4.9338	3.38	2406.9	0	9.750×10^{23}	8.06×10^{25}
1.5913	10.47	107.3	1	1.099×10^{26}	2.90×10^{26}
1.8306	9.10	142.0	1	5.724×10^{25}	5.18×10^{26}
2.0690	8.06	181.4	1	3.278×10^{25}	1.04×10^{27}
2.3872	6.98	241.5	1	1.744×10^{25}	2.65×10^{27}
2.7055	6.16	310.3	1	1.024×10^{25}	5.86×10^{27}
2.9444	5.66	367.6	1	7.255×10^{24}	8.68×10^{27}
3.1829	5.24	429.8	1	5.350×10^{24}	9.68×10^{27}
3.3421	4.99	474.1	1	4.449×10^{24}	6.79×10^{27}
3.5811	4.65	544.9	1	3.474×10^{24}	3.07×10^{27}
3.8196	4.36	620.9	1	2.796×10^{24}	1.19×10^{27}
4.0583	4.11	702.7	1	2.313×10^{24}	6.88×10^{26}
4.2975	3.88	791.0	1	1.973×10^{24}	3.76×10^{26}
4.5369	3.67	887.0	1	1.743×10^{24}	2.12×10^{26}
4.7710	3.49	991.1	1	1.632×10^{24}	1.18×10^{26}
5.0078	3.33	1118.0	1	1.885×10^{24}	6.90×10^{25}
1.9258	8.65	100.0	2	7.715×10^{25}	6.87×10^{26}
2.2489	7.41	100.0	3	5.331×10^{25}	1.77×10^{27}
2.5309	6.59	100.0	4	4.044×10^{25}	4.06×10^{27}
2.7846	5.99	100.0	5	3.263×10^{25}	6.55×10^{27}
3.0169	5.52	100.0	6	2.751×10^{25}	9.32×10^{27}
3.2326	5.16	100.0	7	2.392×10^{25}	9.07×10^{27}
3.4346	4.85	100.0	8	2.131×10^{25}	5.12×10^{27}
3.6254	4.60	100.0	9	1.937×10^{25}	2.58×10^{27}
3.8065	4.38	100.0	10	1.788×10^{25}	1.24×10^{27}
3.9792	4.19	100.0	11	1.672×10^{25}	7.91×10^{26}
4.1446	4.02	100.0	12	1.582×10^{25}	5.72×10^{26}
4.3035	3.87	100.0	13	1.511×10^{25}	3.70×10^{26}
4.4565	3.74	100.0	14	1.458×10^{25}	2.55×10^{26}
4.6042	3.62	100.0	15	1.420×10^{25}	1.80×10^{26}

e) Energy Transfer Rates

We compute net energy transfer rates for a selected sample of modes whose parameters are listed in Table 2. The modes have been chosen to sample the region of $k_h - \omega$ diagram which makes the greatest contribution to mode couplings. Therefore, most lie on the $n = 0$ and $n = 1$ ridges. In addition, we have included modes with fixed $l = 100$ and a range of n values. These are used to gauge the effects of nonlinear interactions on mode energy, line width, and overstability. The computed values of $\Upsilon_\alpha^{(1)}$ and $\Upsilon_\alpha^{(2)}$ are listed in Tables 3 and 4 for two different choices of the thickness of isothermal atmosphere. An obvious feature is that every trapped mode, except the lowest frequency one, is losing energy due to its nonlinear interactions. Of course, class 1 couplings drain energy from trapped modes by transferring it to propagating modes. However, even class 2 couplings, which conserve the energy of the trapped modes, damp all modes expect those in a narrow frequency range bounded from above by ω_{ac}. This is a consequence of the steep decline in the energy per mode as ω approaches ω_{ac} from below.

The lifetimes (the inverses of the line widths) of the low-degree solar p-modes near the peak of the 5 minute band are of order several days (Libbrecht 1988; Libbrecht and Zirin 1986; Isaak 1986). In addition, the mode lifetimes decrease monotonically with increasing ω at fixed k_h. The significance of the nonlinear interactions is measured by comparing the damping rate, $\eta_\alpha \equiv \Upsilon_\alpha/E_\alpha$, displayed in Tables 3 and 4, to the line width for each mode.

The values of η_α are quite sensitive to the thickness of the isothermal layer and to the energies of the high-degree fundamental, $n = 0$, modes. For a thin isothermal layer and small energies of the high-degree modes, the calculated damping times of low-degree,

© American Astronomical Society • Provided by the NASA Astrophysics Data System

1989ApJ...342..558K

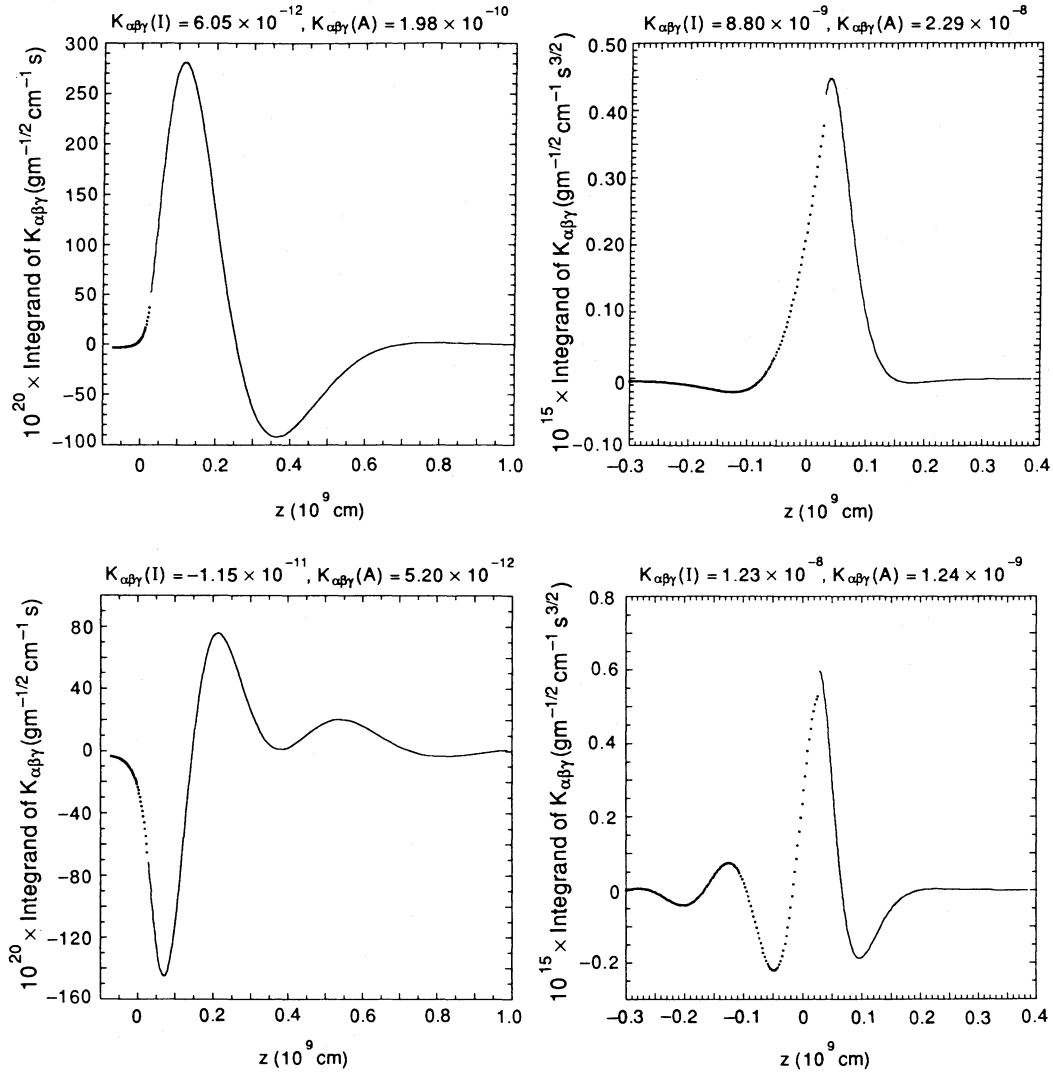

FIG. 3.—Integrand of $K_{\alpha\beta\gamma}$ for four triplets. Solid and dotted lines are used in the adiabatic and isothermal layer, respectively. The isothermal layer is 2.5 scale heights thick. Discontinuity in $K_{\alpha\beta\gamma}$ is due to the discontinuity of $\partial\xi_z/\partial z$. Clockwise from the upper left, the values of ν (mHz) and l for the three modes in each triplet are {(1.5915, 250), (2.1723, 200), (3.7597, 280)}, {(1.5915, 250), (3.8950, 1500), (5.4866, 1400)}, {(3.2308, 100), (1.6828, 120), (4.9155, 185)}, and {(3.2308, 100), (3.8945, 1500), (7.1254, 1400)}. Contributions to the coupling coefficient from the isothermal and adiabatic layer, $K_{\alpha\beta\gamma}(I)$ and $K_{\alpha\beta\gamma}(A)$, are written at the top of each panel. Units are $g^{-1/2} s^{3/2}$ for class 1 triplets (panels 2 and 4) and $g^{-1/2} s$ for class 2 triplets (panels 1 and 3).

5 minute, modes are several months, much longer than the observed lifetimes. However, for a thick isothermal layer and l independent energies, the damping times for these modes drop to several days, close to the values deduced from observation.

The scale length for the exponential growth of the eigenfunctions in the isothermal layer decreases with increasing frequency (see eq. [15]). This accounts for the increase with frequency of the sensitivity of the damping times to the thickness of the isothermal layer.

The values of $\Upsilon_\alpha^{(1)}$ and $\Upsilon_\alpha^{(2)}$ listed in Tables 3 and 4 display a few abrupt changes over small ranges of $k_{h\alpha}$. These are puzzling but do not signal an error in our computations. Rather, they may be traced to the availability or unavailability of triplets which couple mode α to modes on a particular ridge, usually the fundamental, $n = 0$, ridge.

f) *Effect of Mode Couplings on p-Mode Energy Spectrum*

In this section we assume that the excitation of the p-modes is due to the emission of acoustic radiation by turbulent convection. Mode damping is attributed to an unspecified combination of radiative damping and the absorption of acoustic radiation by turbulence. We adopt a crude model for these processes in which we set

$$\left\langle \frac{dE_\alpha}{dt} \right\rangle = A_\alpha - B_\alpha E_\alpha . \tag{54}$$

© American Astronomical Society • Provided by the NASA Astrophysics Data System

1989ApJ...342..558K

TABLE 3

ENERGY DISSIPATION RATE DUE TO MODE COUPLINGS

ν (mHz)	$k_h R_\odot \equiv \ell$	E_α(erg)	$\Upsilon_\alpha^{(1)}$ (erg/sec)	$\Upsilon_\alpha^{(2)}$ (erg/sec)	η_α (sec^{-1})
1.1140	122.7	2.90×10^{26}	-1.33×10^{18}	3.75×10^{18}	8.34×10^{-9}
1.5914	250.4	2.90×10^{26}	-1.14×10^{20}	-6.72×10^{19}	-6.25×10^{-7}
1.7505	303.0	3.94×10^{26}	-2.55×10^{20}	-1.55×10^{20}	-1.04×10^{-6}
1.8620	342.8	5.70×10^{26}	-6.47×10^{20}	-2.28×10^{20}	-1.54×10^{-6}
1.9894	391.3	8.28×10^{26}	-1.38×10^{21}	-2.80×10^{20}	-2.00×10^{-6}
2.2282	490.9	1.66×10^{27}	-4.78×10^{21}	-2.96×10^{20}	-3.06×10^{-6}
2.3873	563.5	2.65×10^{27}	-1.01×10^{22}	-3.07×10^{20}	-3.93×10^{-6}
2.5463	641.1	4.26×10^{27}	-2.13×10^{22}	-2.83×10^{20}	-5.07×10^{-6}
2.7852	767.0	6.56×10^{27}	-4.75×10^{22}	-1.70×10^{20}	-7.27×10^{-6}
3.0239	904.1	9.37×10^{27}	-0.99×10^{23}	-9.14×10^{19}	-1.06×10^{-5}
3.1831	1001.8	9.68×10^{27}	-1.30×10^{23}	-5.76×10^{19}	-1.34×10^{-5}
3.3423	1104.5	6.79×10^{27}	-1.17×10^{23}	-2.06×10^{19}	-1.72×10^{-5}
3.5810	1267.9	3.07×10^{27}	-7.67×10^{22}	-1.00×10^{19}	-2.50×10^{-5}
3.7401	1383.1	1.61×10^{27}	-5.08×10^{22}	0.00	-3.16×10^{-5}
3.9789	1565.3	7.91×10^{26}	-3.65×10^{22}	0.00	-4.61×10^{-5}
4.3768	1894.0	3.07×10^{26}	-2.52×10^{22}	0.00	-8.21×10^{-5}
4.6155	2106.3	1.75×10^{26}	-2.03×10^{22}	0.00	-1.16×10^{-4}
4.9338	2406.9	8.06×10^{25}	-1.48×10^{22}	0.00	-1.84×10^{-4}
1.5913	107.3	2.90×10^{26}	-1.86×10^{19}	-3.26×10^{19}	-1.77×10^{-7}
1.8306	142.0	5.18×10^{26}	-1.02×10^{20}	-3.88×10^{18}	-2.04×10^{-7}
2.0690	181.4	1.04×10^{27}	-3.93×10^{20}	-6.41×10^{19}	-4.40×10^{-7}
2.3872	241.5	2.65×10^{27}	-2.14×10^{21}	-4.24×10^{19}	-8.24×10^{-7}
2.7055	310.3	5.86×10^{27}	-7.47×10^{21}	-2.34×10^{19}	-1.28×10^{-6}
2.9444	367.6	8.68×10^{27}	-1.55×10^{22}	-1.00×10^{19}	-1.79×10^{-6}
3.1829	429.8	9.68×10^{27}	-2.49×10^{22}	-3.71×10^{18}	-2.57×10^{-6}
3.3421	474.1	6.79×10^{27}	-2.25×10^{22}	-1.29×10^{18}	-3.31×10^{-6}
3.5811	544.9	3.07×10^{27}	-1.53×10^{22}	-3.39×10^{17}	-4.98×10^{-6}
3.8196	620.9	1.19×10^{27}	-8.78×10^{21}	-2.32×10^{18}	-7.38×10^{-6}
4.0583	702.7	6.88×10^{26}	-7.53×10^{21}	1.25×10^{18}	-1.09×10^{-5}
4.2975	791.0	3.76×10^{26}	-6.05×10^{21}	2.57×10^{19}	-1.60×10^{-5}
4.5369	887.0	2.12×10^{26}	-5.37×10^{21}	1.38×10^{20}	-2.47×10^{-5}
4.7710	991.1	1.18×10^{26}	-4.90×10^{21}	5.95×10^{20}	-3.65×10^{-5}
5.0078	1118.0	6.90×10^{25}	-5.76×10^{21}	2.57×10^{21}	-4.62×10^{-5}
1.9258	100.0	6.87×10^{26}	-9.82×10^{19}	-2.12×10^{18}	-1.46×10^{-7}
2.2489	100.0	1.77×10^{27}	-4.09×10^{20}	-1.69×10^{19}	-2.41×10^{-7}
2.5309	100.0	4.06×10^{27}	-1.22×10^{21}	-7.78×10^{18}	-3.02×10^{-7}
2.7846	100.0	6.55×10^{27}	-2.43×10^{21}	-2.66×10^{18}	-3.71×10^{-7}
3.0169	100.0	9.32×10^{27}	-4.18×10^{21}	-5.60×10^{17}	-4.49×10^{-7}
3.2326	100.0	9.07×10^{27}	-4.80×10^{21}	-1.36×10^{17}	-5.29×10^{-7}
3.4346	100.0	5.12×10^{27}	-3.08×10^{21}	-2.41×10^{16}	-6.02×10^{-7}
3.6254	100.0	2.58×10^{27}	-1.78×10^{21}	-5.89×10^{15}	-6.90×10^{-7}
3.8065	100.0	1.24×10^{27}	-1.00×10^{21}	-6.01×10^{15}	-8.06×10^{-7}
3.9792	100.0	7.91×10^{26}	-7.73×10^{20}	-1.50×10^{15}	-9.77×10^{-7}
4.1446	100.0	5.72×10^{26}	-7.06×10^{20}	7.48×10^{15}	-1.23×10^{-6}
4.3035	100.0	3.70×10^{26}	-5.92×10^{20}	3.76×10^{16}	-1.60×10^{-6}
4.4565	100.0	2.55×10^{26}	-5.28×10^{20}	1.31×10^{17}	-2.07×10^{-6}
4.6042	100.0	1.80×10^{26}	-4.79×10^{20}	3.61×10^{17}	-2.66×10^{-6}

Here A_α denotes the mean rate of turbulent excitation and B_α expresses the damping due to radiation and turbulence. We assume that both A_α and B_α are inversely proportional to $\mathcal{M}_\alpha$. Therefore, in the absence of mode couplings all modes have the same energy.[8] We include the effect of the dominant, class 1, mode couplings on the energy spectrum by adding equation (47) to equation (54) to obtain

$$\frac{dE_\alpha}{dt} = A_\alpha - B_\alpha E_\alpha + \frac{9\omega_\alpha}{2\pi} \sum_{n_\beta,\,\gamma_{s\gamma}} \int dk_{h\beta}\, k_{h\beta} \int_0^\pi d\theta_{\alpha\beta}\, |K_{\alpha_{s\alpha}\beta_{s\beta}\gamma_{s\gamma}}|^2\, \delta(\omega_\alpha + s_1\omega_\beta + s_2\omega_\gamma)(\omega_\alpha E_\beta E_\gamma + s_1\omega_\beta E_\alpha E_\gamma + s_2\omega_\gamma E_\alpha E_\beta)\,. \quad (55)$$

The above set of coupled equations is solved to yield the equilibrium energies of the modes. The result for low-l modes is shown in Figure 4 and for modes on $n = 0$ and 1 ridges is contained in Table 5. Note that the three-mode couplings reduce all of the mode energies, with the largest effect occurring for the highest values of $\omega < \omega_{ac}$ and k_h. In addition, the energy spectrum has developed a peak at a frequency of $\sim$4.0 mHz.

It is not obvious how mode couplings produce a peak in the energy spectrum which in their absence would be flat. This effect has its roots in the geometry of $k_h - \omega$ diagram, and is best understood by reference to pseudomodes. Modes of fixed $l = 100$ and

[8] Numerical values for A_α and B_α are set by adopting 1.0 μHz and 5.0×10^{27} ergs for the line width and energy of the 5 minute radial mode.

© American Astronomical Society • Provided by the NASA Astrophysics Data System

1989ApJ...342..558K

TABLE 4

ENERGY DISSIPATION RATE DUE TO MODE COUPLINGS

ν (mHz)	$k_h R_\odot \equiv \ell$	E_α(erg)	$\Upsilon_\alpha^{(1)}$ (erg/sec)	$\Upsilon_\alpha^{(2)}$ (erg/sec)	η_α (sec^{-1})
1.1140	122.7	2.90×10^{26}	-2.20×10^{18}	3.75×10^{18}	5.34×10^{-9}
1.5914	250.4	2.90×10^{26}	-1.36×10^{20}	-7.43×10^{19}	-7.25×10^{-7}
1.7505	303.0	3.94×10^{26}	-2.81×10^{20}	-1.69×10^{20}	-1.14×10^{-6}
1.8620	342.8	5.70×10^{26}	-6.93×10^{20}	-2.56×10^{20}	-1.66×10^{-6}
1.9894	391.3	8.28×10^{26}	-1.40×10^{21}	-3.14×10^{20}	-2.07×10^{-6}
2.2282	490.9	1.66×10^{27}	-4.69×10^{21}	-3.34×10^{20}	-3.03×10^{-6}
2.3873	563.5	2.65×10^{27}	-0.99×10^{22}	-3.50×10^{20}	-3.88×10^{-6}
2.5463	641.1	4.26×10^{27}	-2.13×10^{22}	-3.25×10^{20}	-5.08×10^{-6}
2.7852	767.0	6.56×10^{27}	-4.73×10^{22}	-1.94×10^{20}	-7.24×10^{-6}
3.0239	904.1	9.37×10^{27}	-9.38×10^{22}	-1.05×10^{20}	-1.00×10^{-5}
3.1831	1001.8	9.68×10^{27}	-1.20×10^{23}	-6.55×10^{19}	-1.24×10^{-5}
3.3423	1104.5	6.79×10^{27}	-1.08×10^{23}	-2.25×10^{19}	-1.59×10^{-5}
3.5810	1267.9	3.07×10^{27}	-6.86×10^{22}	-1.11×10^{19}	-2.23×10^{-5}
3.7401	1383.1	1.61×10^{27}	-4.61×10^{22}	0.00	-2.86×10^{-5}
3.9789	1565.3	7.91×10^{26}	-3.28×10^{22}	0.00	-4.15×10^{-5}
4.3768	1894.0	3.07×10^{26}	-2.54×10^{22}	0.00	-8.27×10^{-5}
4.6155	2106.3	1.75×10^{26}	-2.31×10^{22}	0.00	-1.32×10^{-4}
4.9338	2406.9	8.06×10^{25}	-2.10×10^{22}	0.00	-2.61×10^{-4}
1.5913	107.3	2.90×10^{26}	-2.36×10^{19}	-3.65×10^{19}	-2.07×10^{-7}
1.8306	142.0	5.18×10^{26}	-1.07×10^{20}	-5.31×10^{18}	-2.17×10^{-7}
2.0690	181.4	1.04×10^{27}	-3.55×10^{20}	-7.34×10^{19}	-4.12×10^{-7}
2.3872	241.5	2.65×10^{27}	-1.84×10^{21}	-4.90×10^{19}	-7.13×10^{-7}
2.7055	310.3	5.86×10^{27}	-5.88×10^{21}	-2.76×10^{19}	-1.01×10^{-6}
2.9444	367.6	8.68×10^{27}	-1.20×10^{22}	-1.17×10^{19}	-1.38×10^{-6}
3.1829	429.8	9.68×10^{27}	-1.94×10^{22}	-4.24×10^{18}	-2.00×10^{-6}
3.3421	474.1	6.79×10^{27}	-1.74×10^{22}	-1.46×10^{18}	-2.56×10^{-6}
3.5811	544.9	3.07×10^{27}	-1.09×10^{22}	-3.74×10^{17}	-3.55×10^{-6}
3.8196	620.9	1.19×10^{27}	-5.92×10^{21}	-2.34×10^{18}	-4.98×10^{-6}
4.0583	702.7	6.88×10^{26}	-5.36×10^{21}	1.26×10^{18}	-7.79×10^{-6}
4.2975	791.0	3.76×10^{26}	-4.95×10^{21}	2.59×10^{19}	-1.31×10^{-5}
4.5369	887.0	2.12×10^{26}	-5.08×10^{21}	1.39×10^{20}	-2.33×10^{-5}
4.7710	991.1	1.18×10^{26}	-6.49×10^{21}	6.08×10^{20}	-4.98×10^{-5}
5.0078	1118.0	6.90×10^{25}	-1.30×10^{22}	2.65×10^{21}	-1.50×10^{-4}
1.9258	100.0	6.87×10^{26}	-1.03×10^{20}	-2.22×10^{18}	-1.53×10^{-7}
2.2489	100.0	1.77×10^{27}	-3.56×10^{20}	-2.01×10^{19}	-2.12×10^{-7}
2.5309	100.0	4.06×10^{27}	-9.55×10^{20}	-1.01×10^{19}	-2.38×10^{-7}
2.7846	100.0	6.55×10^{27}	-1.68×10^{21}	-3.36×10^{18}	-2.57×10^{-7}
3.0169	100.0	9.32×10^{27}	-2.53×10^{21}	-6.94×10^{17}	-2.72×10^{-7}
3.2326	100.0	9.07×10^{27}	-2.64×10^{21}	-1.76×10^{17}	-2.91×10^{-7}
3.4346	100.0	5.12×10^{27}	-1.74×10^{21}	-3.12×10^{16}	-3.40×10^{-7}
3.6254	100.0	2.58×10^{27}	-1.17×10^{21}	-7.17×10^{15}	-4.53×10^{-7}
3.8065	100.0	1.24×10^{27}	-7.84×10^{20}	-6.47×10^{15}	-6.32×10^{-7}
3.9792	100.0	7.91×10^{26}	-6.76×10^{20}	-1.58×10^{15}	-8.55×10^{-7}
4.1446	100.0	5.72×10^{26}	-6.19×10^{20}	8.53×10^{15}	-1.08×10^{-6}
4.3035	100.0	3.70×10^{26}	-4.76×10^{20}	4.60×10^{16}	-1.29×10^{-6}
4.4565	100.0	2.55×10^{26}	-3.85×10^{20}	1.70×10^{17}	-1.51×10^{-6}
4.6042	100.0	1.80×10^{26}	-3.44×10^{20}	5.11×10^{17}	-1.91×10^{-6}

$\nu \lesssim 3.0$ mHz couple most strongly to mode pairs consisting of a trapped mode on the f-ridge and a pseudomode on the $n = 1$ ridge. The l-values of these modes typically fall in a segment of length $\Delta l \sim 400$. The central l-value of the segment increases with increasing $\nu \lesssim 3$ mHz, resulting in an increase in the dissipation rate. For $\nu \sim 4$ mHz, one end of the segment is at $l \sim 3000$ which is where the f-mode ridge terminates. Modes with $l = 100$ and $\nu \gtrsim 4.0$ mHz are most strongly coupled to mode pairs consisting of a trapped mode on the f-ridge and a pseudomode on the $n = 2$ ridge. Therefore, for ν in the range of 3–4 mHz, where a transition from $n = 1$ to $n = 2$ coupling occurs, the dissipation rate is much smaller than that for $\nu \lesssim 3$ mHz. With further increase in $\nu \gtrsim 4$ mHz, modes with $l = 100$ couple to (f-mode, $n = 2$ mode) pairs with higher l, and the dissipation rate again increases with increasing ν. Thus, the peak in the computed energy spectrum is accounted for by the termination of the f-mode ridge near $l = 3000$.

The position of the peak in the energy spectrum is essentially determined by the frequency separation between the $n = 0$ and $n = 1$ ridges at $l \sim 3000$. This separation is ~ 1 mHz larger for our model than it is for the Sun. Therefore, we expect that a similar calculation for a solar model would give rise to a peak in the energy spectrum at $\nu \sim 3$ mHz.

We note that mode couplings give rise to a constant line width near the low-frequency side of the peak, and a constant value for the product of energy and line width on the high-frequency side (see Table 5). Both of these properties are found to hold observationally (Libbrecht 1988). However, the residual uncertainties in our calculations are such that the significance of these qualitative similarities between theory and observation is, at most, suggestive.

© American Astronomical Society • Provided by the NASA Astrophysics Data System

1989ApJ...342..558K

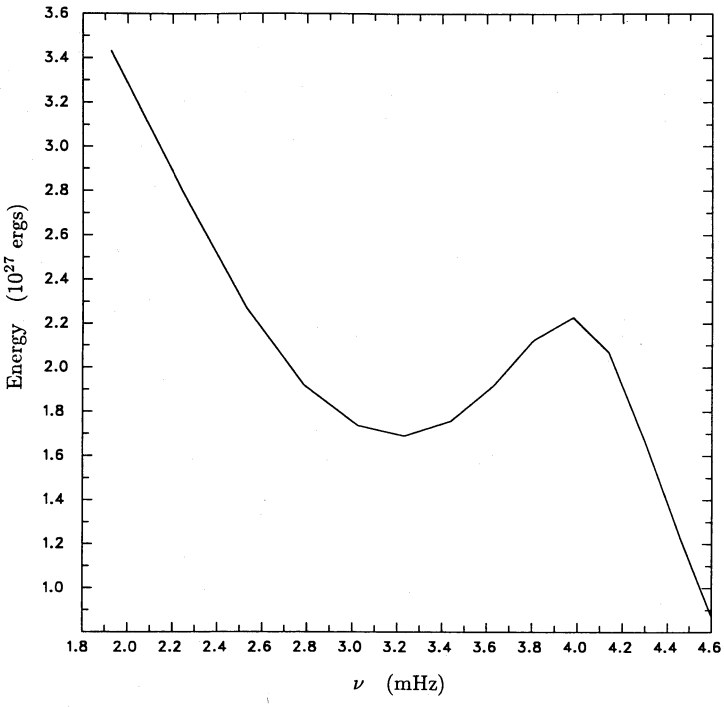

FIG. 4.—Equilibrium energy. Modified energy spectrum due to mode couplings.

g) Error Tests

The energy transfer rates are the end product of a fairly long series of calculations. Their numerical values are the major result of our investigation, and we have tried to ensure that they are correct. In order to minimize the chances for errors, we devised and performed a set of tests of various parts of the calculations.

Approximate analytic eigenfunctions were derived to check the eigenfunctions determined by the numerical solution of the differential equations (1) and (10). These analytic eigenfunctions were used to compute three-mode coupling coefficients, $K_{\alpha\beta\gamma}$, which were compared to those computed from the numerical eigenfunctions.

In our calculations of $\Upsilon_\alpha^{(1)}$ and $\Upsilon_\alpha^{(2)}$, we varied the number of choices of mode β for a given mode α. We also interchanged the roles of modes β and γ in these calculations. Finally, we summed $\Upsilon_\alpha^{(2)}$ over all the trapped modes to verify that the class 2 couplings conserve the total energy in the trapped modes.

V. DISCUSSION AND CONCLUSIONS

a) Significance of Nonlinear Mode Coupling

Nonlinear interactions transfer energy among the normal modes. The most important nonlinear interactions are those which couple two trapped modes to a propagating mode. These drain the energies of the trapped modes. As a consequence, all of the trapped modes, except the lowest frequency ones, suffer a net loss of energy due to nonlinear mode interactions.

These calculated damping times due to mode coupling may be compared to the observationally determined lifetimes of the solar *p*-modes. Unfortunately, this comparison is currently restricted by lack of adequate observational data to low-degree modes near the peak of the 5 minute band. Moreover, there are significant residual uncertainties in the nonlinear damping rates associated with the upper limit we choose for the integrals which give the divergent coupling coefficients, and with the energies we adopt for the high-degree trapped modes. These uncertainties preclude our reaching any firm conclusion regarding the importance of nonlinear interactions in affecting the energies of the solar *p*-modes.

The observational consequences of the three-mode couplings, if they are significant, follow from the dependence of the damping rates on l and ω. The increase in damping rate with increasing l might give rise to a decline of the energy per mode with increasing l at fixed ω. Furthermore, the rapid increase in damping rate as ω approaches ω_{ac} from below might be, at least in part, responsible for the steep decline in the energy per mode at the high-frequency end of the 5 minute band. This decline is generally attributed to radiative damping, but calculations of that process are not secure enough to rule out the existence of another, possibly dominant, contributor.

b) Stabilizing Overstable Modes by Three-Mode Couplings

More than 25 years after the discovery of the 5 minute oscillations by Leighton, Noyes, and Simon (1961) and Evans and Michard (1962), we are still uncertain as to how the *p*-modes are excited. There are two leading contenders for the excitation mechanism: self excitation by the opacity (κ) mechanism (Ando and Osaki 1975; Goldreich and Keeley 1977*a*), and stochastic excitation by turbulent convection (Goldreich and Keeley 1977*b*). Unfortunately, neither observation nor theory has been able to establish which, if either, is the correct choice. The linear stability of the solar *f*- and *p*-modes is unresolved despite several theoretical investigations

© American Astronomical Society • Provided by the NASA Astrophysics Data System

1989ApJ...342..558K

TABLE 5

MODIFICATION TO ENERGY SPECTRUM DUE TO MODE COUPLINGS

ν (mHz)	n	$k_h R_\odot \equiv \ell$	E_α(erg)	Γ_α (sec^{-1})	B_α (sec^{-1})
1.1141	0	122.7	4.59×10^{27}	1.93×10^{-7}	1.77×10^{-7}
1.5915	0	250.4	2.60×10^{27}	1.83×10^{-6}	9.53×10^{-7}
1.7507	0	303.0	2.28×10^{27}	3.23×10^{-6}	1.47×10^{-6}
1.8621	0	342.8	2.10×10^{27}	4.63×10^{-6}	1.95×10^{-6}
1.9894	0	391.3	1.98×10^{27}	6.60×10^{-6}	2.62×10^{-6}
2.2282	0	490.9	1.97×10^{27}	1.09×10^{-5}	4.29×10^{-6}
2.3873	0	563.5	2.12×10^{27}	1.36×10^{-5}	5.75×10^{-6}
2.5465	0	641.1	2.27×10^{27}	1.66×10^{-5}	7.53×10^{-6}
2.7852	0	767.0	2.15×10^{27}	2.52×10^{-5}	1.09×10^{-5}
3.0239	0	904.1	1.80×10^{27}	4.16×10^{-5}	1.50×10^{-5}
3.1831	0	1001.8	1.72×10^{27}	5.32×10^{-5}	1.83×10^{-5}
3.3423	0	1104.5	1.71×10^{27}	6.43×10^{-5}	2.20×10^{-5}
3.5810	0	1267.9	1.49×10^{27}	9.54×10^{-5}	2.83×10^{-5}
3.7401	0	1383.1	1.41×10^{27}	1.18×10^{-4}	3.31×10^{-5}
3.9789	0	1565.3	1.23×10^{27}	1.68×10^{-4}	4.11×10^{-5}
4.3768	0	1894.0	9.74×10^{26}	2.91×10^{-4}	5.67×10^{-5}
4.6155	0	2106.3	8.36×10^{26}	4.03×10^{-4}	6.74×10^{-5}
4.9338	0	2406.9	6.58×10^{26}	6.32×10^{-4}	8.32×10^{-5}
1.5915	1	107.3	3.86×10^{27}	3.24×10^{-7}	2.50×10^{-7}
1.8303	1	142.0	3.23×10^{27}	7.45×10^{-7}	4.81×10^{-7}
2.0690	1	181.4	2.69×10^{27}	1.57×10^{-6}	8.42×10^{-7}
2.3873	1	241.5	2.19×10^{27}	3.63×10^{-6}	1.59×10^{-6}
2.7056	1	310.3	2.04×10^{27}	6.69×10^{-6}	2.73×10^{-6}
2.9444	1	367.6	2.13×10^{27}	9.11×10^{-6}	3.88×10^{-6}
3.1831	1	429.8	2.22×10^{27}	1.20×10^{-5}	5.31×10^{-6}
3.3423	1	474.1	2.15×10^{27}	1.50×10^{-5}	6.44×10^{-6}
3.5810	1	544.9	1.83×10^{27}	2.29×10^{-5}	8.38×10^{-6}
3.8197	1	620.9	1.49×10^{27}	3.57×10^{-5}	1.06×10^{-5}
4.0585	1	702.7	1.31×10^{27}	5.06×10^{-5}	1.32×10^{-5}
4.2972	1	791.0	1.16×10^{27}	6.92×10^{-5}	1.61×10^{-5}
4.5359	1	887.0	8.82×10^{26}	1.09×10^{-4}	1.93×10^{-5}
4.7746	1	991.1	6.41×10^{26}	1.77×10^{-4}	2.26×10^{-5}
5.0134	1	1118.0	3.81×10^{26}	3.45×10^{-4}	2.63×10^{-5}
1.9258	2	100.0	3.43×10^{27}	5.20×10^{-7}	3.57×10^{-7}
2.2441	3	100.0	2.80×10^{27}	9.23×10^{-7}	5.17×10^{-7}
2.5306	4	100.0	2.27×10^{27}	1.50×10^{-6}	6.82×10^{-7}
2.7852	5	100.0	1.92×10^{27}	2.20×10^{-6}	8.46×10^{-7}
3.0239	6	100.0	1.74×10^{27}	2.89×10^{-6}	1.01×10^{-6}
3.2308	7	100.0	1.69×10^{27}	3.42×10^{-6}	1.16×10^{-6}
3.4377	8	100.0	1.76×10^{27}	3.70×10^{-6}	1.30×10^{-6}
3.6287	9	100.0	1.92×10^{27}	3.73×10^{-6}	1.43×10^{-6}
3.8038	10	100.0	2.12×10^{27}	3.66×10^{-6}	1.55×10^{-6}
3.9789	11	100.0	2.23×10^{27}	3.73×10^{-6}	1.66×10^{-6}
4.1380	12	100.0	2.07×10^{27}	4.26×10^{-6}	1.76×10^{-6}
4.2972	13	100.0	1.67×10^{27}	5.54×10^{-6}	1.85×10^{-6}
4.4563	14	100.0	1.23×10^{27}	7.82×10^{-6}	1.92×10^{-6}
4.5996	15	100.0	8.72×10^{26}	1.14×10^{-5}	1.98×10^{-6}
4.5996	15	100.0	8.72×10^{26}	1.14×10^{-5}	1.98×10^{-6}

aimed at providing a conclusive answer (Ando and Osaki 1975; Goldreich and Keeley 1977*a*; Christensen-Dalsgaard and Frandsen 1982; Antia, Chitre, and Narashima 1986; Kidman and Cox 1984). Its resolution must await significant advances in modeling the interaction of turbulent convection with pulsation, and in treating radiative transfer in the transition region between high and low optical depth. The inconclusive nature of previous stability calculations is apparent; small and uncertain effects control the delicate balance between stability and overstability. Calculations of the stochastic excitation of the solar modes are plagued by the lack of an adequate theory for the interaction of acoustic radiation with turbulence, although there is encouraging recent progress on this front (Goldreich and Kumar 1988).

Given the current situation it is not clear how best to proceed to determine the mechanism responsible for the excitation of the *p*-modes. An alternative to refining the stability calculations or the theory of the interaction of acoustic radiation with turbulence is to assume that the modes are either stable or overstable and then to explore the implications of each assumption. As discussed below, this approach suggests that knowledge of the rates at which nonlinear interactions transfer energy among the normal modes would indirectly help to resolve the issue of mode stability.

If we assume that at least some of the *p*-modes are linearly overstable, there must be a nonlinear mechanism which saturates the instability and accounts for the observed amplitudes of the modes. An obvious possibility is that overstable modes transfer energy to

© American Astronomical Society • Provided by the NASA Astrophysics Data System

1989ApJ...342..558K

damped modes. The lowest order mode couplings involve near-resonant mode triplets. In order to serve as an amplitude limiting process, these three-mode couplings must be able to drain the energy from the overstable modes on their linear e-folding time scales.

If the solar p-modes are linearly stable, they probably owe their excitation to the emission of acoustic radiation by turbulence near the top of the Sun's convection zone. In that case, their damping is likely due to a combination of acoustic readsorption by the turbulence and radiative diffusion. The three-mode couplings are less crucial if the p-modes are stable. However, they still act to redistribute energy among the different modes. This raises the question of whether an individual mode is more strongly coupled to the turbulent convection or to other acoustic modes.

Our calculations show that the energy decay rates due to mode couplings are, with significant residual uncertainties, probably smaller than the products of the observed line widths and energies of the p-modes in the 5 minute band. By itself, this is a marginal indication that overstable modes could not be stabilized by mode couplings. However, there is better argument against overstable modes. The strongest nonlinear couplings of each f- and p-mode involve modes on the $n = 0$ (f-modes) ridge; the coupling strengths decrease rapidly with increasing n due to effects explained in § IVd. Figure 5 displays the contribution to the coupling coefficient for two different modes α and $n_\beta = 0$, 1 as a function of l_β. This contribution generally increases with increasing l_β until either no more pseudomodes γ are found or $\omega_\beta \geq \omega_{ac}$. It is also evident that the coupling strengths decrease in going from the $n_\beta = 0$ to the $n_\beta = 1$ ridge. To interpret these trends note that the maximum value of k_h on a ridge is proportional to $(n + \frac{3}{4})^{-1}$. Hence the coupling coefficient decreases as $(n + \frac{3}{4})^{-2}$, and the available phase space also decreases as $(n + \frac{3}{4})^{-2}$. This implies that the contribution to η_α from ridge n decreases as $(n + \frac{3}{4})^{-6}$, so for $n_\alpha > 0$, η_α is independent of E_α, but is proportional to the energies of the modes on the fundamental ridge.

If the choice of l independent mode energies has led us to seriously overestimate the energies of the high-l f-modes, the most important couplings might involve the next higher available ridge. This would not affect our conclusion that η_α is independent of E_α for low-l, high-n, p-modes.

The arguments presented above convince us that three-mode couplings, previously considered the best candidate for saturating

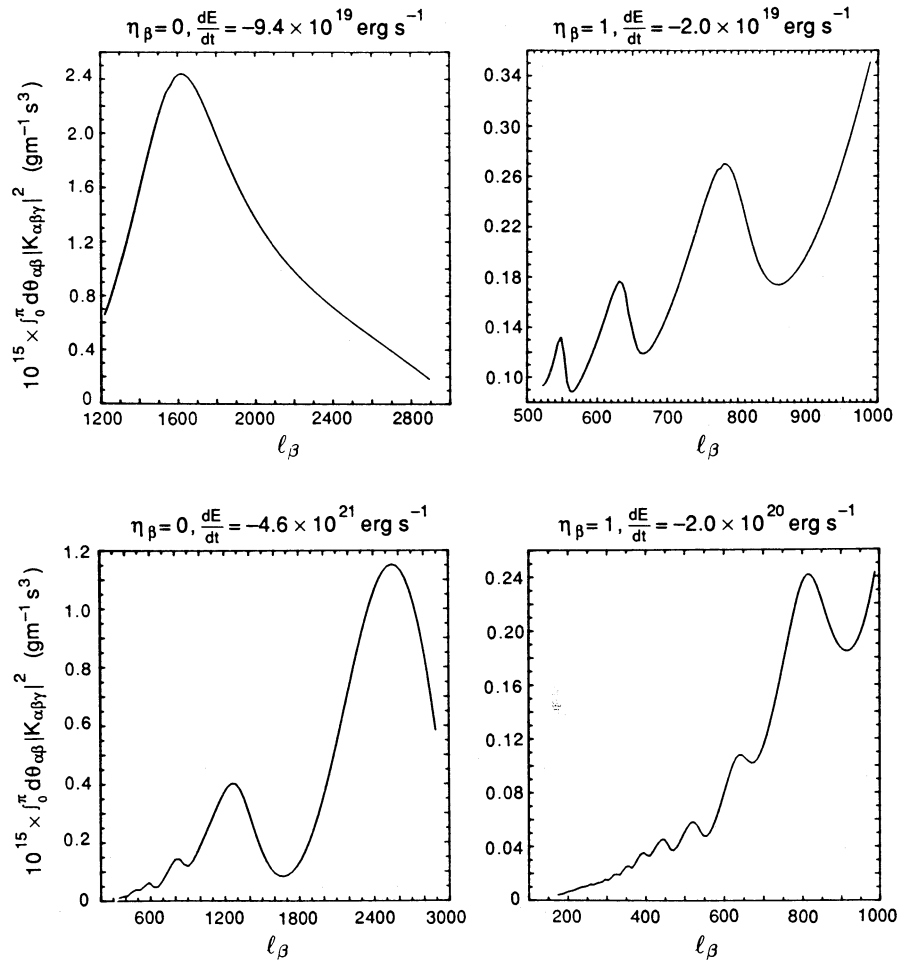

FIG. 5.—Contributions to $|K_{\alpha\beta\gamma}|^2$ from different ridges. Top two graphs are for $n_\alpha = 0$, $\nu_\alpha = 1.591$ mHz, with $n_\beta = 0$ for the left panel and $n_\beta = 1$ for the right panel. Bottom graphs apply for $n_\alpha = 7$, $\nu_\alpha = 3.231$ mHz, with the same values of n_β as for the corresponding panels of the upper graphs.

© American Astronomical Society • Provided by the NASA Astrophysics Data System

1989ApJ...342..558K

the energies of overstable solar p-modes, are not viable for this purpose. This result casts severe doubt on any proposal for overstable p-modes. Recent observational results (Kaufman 1988) indicate that the energies of high-l solar f-modes are comparable to those of p-modes with the same frequency. Since the Lagrangian pressure perturbation almost vanishes for f-modes, it is unlikely that they would be overstable due to opacity mechanism.

The research reported here was supported by a visiting scientist fellowship awarded to P. K. at HAO, and by NSF grant AST 861299 and NASA grant NAGW 1303. We are grateful to Ken Libbrecht for scientific discussions and for providing observational data in advance of publication. We thank Tim Brown and Douglas Gough for making useful comments on an earlier version of the manuscript, and an anonymous referee for suggesting several improvements in our presentation. P. K. is indebted to Lynne Andrade and Vic Tisone for help with the computations that were performed on the Cray-1 at NCAR.

APPENDIX

The equations of inviscid fluid dynamics of a perfect gas with adiabatic index Γ follow from varying the Lagrangian (Newcomb 1962):

$$L = \int d\boldsymbol{x}_0\, \rho_0(\boldsymbol{x}_0)\left[\frac{v^2}{2} - \frac{p(\boldsymbol{x})}{(\Gamma-1)\rho(\boldsymbol{x})} - \psi(\boldsymbol{x})\right]. \tag{A1}$$

The background configuration is specified by $\rho_0(\boldsymbol{x}_0)$, $p_0(\boldsymbol{x}_0)$ and $\boldsymbol{v}_0 = 0$. The variation is achieved by displacing the position of each fluid element from $\boldsymbol{x}_0$ to $\boldsymbol{x} = \boldsymbol{x}_0 + \boldsymbol{\xi}$, where $\boldsymbol{\xi}$ is the Lagrangian displacement. The conservation laws of mass and entropy imply

$$\rho\, d\boldsymbol{x} = \rho_0\, d\boldsymbol{x}_0 \Rightarrow \rho = \rho_0\, \mathcal{J}^{-1}, \tag{A2}$$

and

$$p\rho^{-\Gamma} = p_0\, \rho_0^{-\Gamma} \Rightarrow p = p_0\, \mathcal{J}^{-\Gamma}, \tag{A3}$$

where $\mathcal{J}$ is the Jacobian of the transformation. The Lagrangian can be written in terms of $\mathcal{J}$ and the background variables as

$$L = \int d\boldsymbol{x}_0\, \rho_0\left[\frac{v^2}{2} - \frac{p_0\, \mathcal{J}^{1-\Gamma}}{\rho_0(\Gamma-1)} - \psi(\boldsymbol{x}_0 + \boldsymbol{\xi})\right]. \tag{A4}$$

The Jacobian

$$\mathcal{J} = \det\left(\frac{\partial \boldsymbol{x}}{\partial \boldsymbol{x}_0}\right) = \det\left(1 + \frac{\partial \boldsymbol{\xi}}{\partial \boldsymbol{x}_0}\right) \tag{A5}$$

may be rewritten in mixed vector and Cartesian tensor notation as

$$\mathcal{J} = 1 + (\nabla\cdot\boldsymbol{\xi}) - \frac{1}{2}\,\xi^{i,j}\xi^{j,i} + \frac{1}{2}(\nabla\cdot\boldsymbol{\xi})^2 + \frac{1}{3}\,\xi^{i,j}\xi^{j,k}\xi^{k,i} - \frac{(\nabla\cdot\boldsymbol{\xi})}{2}\,\xi^{i,j}\xi^{j,i} + \frac{1}{6}(\nabla\cdot\boldsymbol{\xi})^3, \tag{A6}$$

where $\xi^{i,j}$ is the derivative of ξ^i with respect to x^j, and the summation convection for repeated indices as assumed. Expanding the Lagrangian in powers of the displacement, $\boldsymbol{\xi}$, with the aid of equation (A6), we obtain the second- and third-order Lagrangian densities,

$$\mathcal{L}_2 = \frac{\rho_0}{2}\left|\frac{\partial \boldsymbol{\xi}}{\partial t}\right|^2 - \frac{p_0}{2}\left[(\Gamma-1)(\nabla\cdot\boldsymbol{\xi})^2 + \xi^{i,j}\xi^{j,i}\right] - \frac{\rho_0}{2}\,\psi_{,ij}\,\xi_i\,\xi_j, \tag{A7}$$

and

$$\mathcal{L}_3 = p_0\left[\frac{(\Gamma-1)^2}{6}(\nabla\cdot\boldsymbol{\xi})^3 + \frac{(\Gamma-1)}{2}(\nabla\cdot\boldsymbol{\xi})\xi^{i,j}\xi^{j,i} + \frac{1}{3}\,\xi^{i,j}\xi^{j,k}\xi^{k,i}\right] - \frac{\rho_0}{6}\,\psi_{,ijk}\,\xi_i\,\xi_j\,\xi_k. \tag{A8}$$

The final terms in $\mathcal{L}_2$ and $\mathcal{L}_3$ vanish for a uniform gravitational field.

The Hamiltonian and Lagrangian densities are related by

$$\mathcal{H} = \frac{\delta\mathcal{L}}{\delta\partial_t\xi_i}\,\partial_t\xi_i - \mathcal{L}. \tag{A9}$$

Using equations (A7), (A8) and (A9), we derive the second- and third-order Hamiltonian densities,

$$\mathcal{H}_2 = \frac{\rho_0}{2}\left|\frac{\partial \boldsymbol{\xi}}{\partial t}\right|^2 + \frac{p_0}{2}\left[(\Gamma-1)(\nabla\cdot\boldsymbol{\xi})^2 + \xi^{i,j}\xi^{j,i}\right], \tag{A10}$$

and

$$\mathcal{H}_3 = -\mathcal{L}_3. \tag{A11}$$

© American Astronomical Society • Provided by the NASA Astrophysics Data System

1989ApJ...342..558K

REFERENCES

Ando, H., and Osaki, Y. 1975, *Pub. Astr. Soc. Japan*, **27**, 581.
Antia, H. M., Chitre, S. M., and Narashima, D. 1986, *Ap. Space Sci.*, **118**, 169.
Christensen-Dalsgaard, J. 1980, *M.N.R.A.S.*, **190**, 765.
Christensen-Dalsgaard, J., and Frandsen, S. 1982, *Solar Phys.*, **82**, 165.
Christensen-Dalsgaard, J., and Gough, D. O. 1980, *Nature*, **288**, 544.
Dziembowski, W. 1982, *Act. Astr.*, **32**, 147.
Evans, J. W., and Michard, R. 1962, *Ap. J.*, **136**, 493.
Goldreich, P., and Keeley, D. A. 1977*a*, *Ap. J.*, **211**, 934.
———. 1977*b*, *Ap. J.*, **212**, 243.
Goldreich, P., and Kumar, P. 1988, *Ap. J.*, **326**, 462.
Isaak, G. R. 1986, in *Seismology of the Sun and the Distant Stars*, ed. D. O. Gough (Dordrecht: Reidel), p. 223.
Kaufman, J. M. 1988, Caltech preprint.
Kidman, R. B., and Cox, A. N. 1984, in *Solar Seismology from Space*, ed. R. K. Ulrich, J. Harvey, E. J. Rhodes, Jr., and J. Toomre (JPL Pub. 84–84), p. 335.
Leighton, R. B., Noyes, R. W., and Simon, G. W. 1961, *Ap. J.*, **135**, 474.
Libbrecht, K. G. 1988, *Ap. J.*, **334**, 510.
Libbrecht, K. G., Popp, B. D., Kaufman, J. M., and Penn, M. J. 1986, *Nature*, **323**, 235.
Libbrecht, K. G., and Zirin, H. 1986, *Ap. J.*, **308**, 413.
Newcomb, W. A. 1962, *Nuclear Fusion: Supplement Part 2* (Vienna: International Atomic Energy Agency), p. 451.
Spiegel, E. A., and Unno, W. 1962, *Pub. Astr. Soc. Japan* **14**, 28.
Wentzel, D. G. 1987, *Ap. J.*, **319**, 966.

PETER GOLDREICH: California Institute of Technology, Mail stop 170-25, Geology and Planetary Physics, Pasadena, CA 91125

PAWAN KUMAR: High Altitude Observatory, NCAR, P.O. Box 3000, Boulder, CO 80307

© American Astronomical Society • Provided by the NASA Astrophysics Data System